Thesis No: CSER-M-22-12

A Study on Hemoglobin and Glucose Levels Estimation Techniques Using Optimal PPG Characteristic Features of Smartphone Videos

by

S. M. Taslim Uddin Raju

A thesis submitted in partial fulfillment of the requirements for the degree of
Master of Science in Computer Science & Engineering

Department of Computer Science and Engineering
Khulna University of Engineering & Technology
Khulna-9203, Bangladesh

December 2022

A Study on Hemoglobin and Glucose Levels Estimation Techniques Using Optimal PPG Characteristic Features of Smartphone Videos

by

S. M. Taslim Uddin Raju
Roll No: 1907564

A thesis submitted in partial fulfillment of the requirements for the degree of
Master of Science in Computer Science & Engineering

Department of Computer Science and Engineering
Khulna University of Engineering & Technology
Khulna-9203, Bangladesh
December 2022

Declaration

This is to certify that the thesis work entitled "A Study on Hemoglobin and Glucose Levels Estimation Techniques Using Optimal PPG Characteristic Features of Smartphone Videos" has been carried out by S. M. Taslim Uddin Raju in the Department of Computer Science and Engineering, Khulna University of Engineering & Technology, Khulna, Bangladesh. The above thesis work or any part of this work has not been submitted anywhere for the award of any degree or diploma.

Signature of Supervisor	Signature of Candidate

Approval

This is to certify that the thesis work submitted by S. M. Taslim Uddin Raju entitle "A Study on Hemoglobin and Glucose Levels Estimation Techniques Using Optimal PPG Characteristic Features of Smartphone Videos" has been approved by the board of examiners for the partial fulfillment of the requirements for the degree of Masters of Science in Engineering in the Department of Computer Science & Engineering, Khulna University of Engineering & Technology, Khulna, Bangladesh in December, 2022.

BOARD OF EXAMINERS

1. _____ Chairman
   Dr. M.M.A. Hashem (Supervisor)
   Professor
   Department of Computer Science and Engineering
   Khulna University of Engineering & Technology, Khulna-9203

2. _____ Member
   Head
   Department of Computer Science and Engineering
   Khulna University of Engineering & Technology, Khulna-9203

3. _____ Member
   Dr. K. M. Azharul Hasan
   Professor
   Department of Computer Science and Engineering
   Khulna University of Engineering & Technology, Khulna-9203

4. _____ Member
   Dr. Pintu Chandra Shill
   Professor
   Department of Computer Science and Engineering
   Khulna University of Engineering & Technology, Khulna-9203

5. _____ Member
   Dr. Md. Anisur Rahman (External)
   Professor
   Computer Science & Engineering Discipline
   Khulna University, Khulna

Acknowledgment

At first, I would like to thank almighty Allah for giving all his blessings on me to complete my task. It is my immense pleasure to express my deepest gratitude to my supervisor Dr. M. M. A. Hashem, Professor, Department of Computer Science and Engineering (CSE), Khulna University of Engineering & Technology (KUET) for his continuous encouragement, constant guidance and keen supervision throughout of this study. I will remember his inspiring guidelines in my future. I am also grateful to my parents, and friends for their patience, support and encouragement during this period.

A very special thanks to my beloved wife, Farhana Sultana Taposi for her heartfelt encouragement, cares and helps throughout the entire period of M.Sc. program.

I also wish to thanks the authority of Khulna University of Engineering & Technology, Khulna for providing me with the necessary permission and financial assistance for conducting this thesis work

S. M. Taslim Uddin Raju

Abstract

Blood components such as hemoglobin (Hb), and glucose (Gl) measuring are essential for monitoring one's health condition. Normally, clinical assessments of Hb and Gl are performed by evaluating blood samples collected through venipuncture in laboratories. These techniques are uncomfortable, painful, and costly for patients. A non-invasive, affordable, accurate, and point-of-care Hb and Gl test is required everywhere. This study proposes a novel non-invasive, cost-effective, and convenient method for monitoring Hb and Gl levels using photoplethysmogram (PPG) signal extracted from smartphone video, and deep neural networks (DNN). Fingertip videos are collected from 93 subjects using a smartphone camera and a lighting source, and subsequently the frames are converted into PPG signal. The PPG signals have been preprocessed with Butterworth bandpass filter to eliminate high frequency noise, and motion artifact. Therefore, 34 characteristic features are extracted from the PPG signal and its derivatives and Fourier transformed form. In addition, age and gender are also included as features due to their considerable influence on hemoglobin and glucose. Maximal information coefficient (MIC) feature selection technique has been applied to select the optimal features to avoid redundancy and over-fitting. Finally, DNN based models have been developed to estimate the blood Hb, and Gl levels from the optimal feature set. To compare the performance of the DNN based models, several classical regression models were also developed using the same input condition as DNN based models. A comparison between DNN based models and classical regression models have been done by estimating different error measurement metrics. DNN models along with the MIC feature selection technique outperformed in estimating Hb and Gl levels with the coefficient of determination (R^2) of 0.969 and 0.968, respectively. Experimental outcomes demonstrate that the proposed approach can be utilized clinically to monitor blood component levels without drawing blood samples. This research also shows that smartphone-based PPG signal has the potential to precisely measure the various blood components.

Contents

LIST OF TABLES

LIST OF FIGURES

Nomenclature

Hb	**H**emoglobin
Gl	**G**lucose
NIR-LED	**N**ear **I**nfrared **R**ay **L**ight **E**mitting **D**iode
PPG	**P**hotoplethysmogram
DNN	**D**eep **N**eural **N**etwork
LR	**L**inear **R**egression
SVR	**S**upport **V**ector **R**egression
RFR	**R**andom **F**orest **R**egression
ANN	**A**rtificial **N**eural **N**etwork
PLS	**P**artial **L**east **S**quares
LSR	**L**east **S**quare **R**egression
PCA	**P**rincipal **C**omponent **A**nalysis
MLR	**M**ultivariate **L**inear **R**egression
BWA	**B**isquare **W**eighting **A**lgorithm
CART	**C**lassification **a**nd **R**egression **T**ree
GRNN	**G**eneral **R**egression **N**eural **N**etwork
MLP	**M**ulti **L**ayer **P**erceptron
GLR	**G**eneralized **L**inear **R**egression

CHAPTER I

Introduction

1.1 Background

Blood is the essential life-maintaining fluid that strews over the whole body and is responsible for carrying heat, hormones, antibodies, immune cells, etc. necessary for every cell. Everything related to the life cycle depends on blood directly or indirectly. Hemoglobin (Hb) and glucose (Gl) are two key components of human blood. Hb, a protein molecule is the fundamental element of the red blood cells. Hb carries oxygen around the body from the lungs. Hb is also essential for preserving the structure of red blood cells. Red blood cells are naturally spherical with narrow centers, resembling a doughnut with no hole in the middle. Therefore, abnormal Hb structure can alter the shape of red blood cells and hinder their activity and blood flow within blood vessels. Hb level is expressed as the amount of Hb in grams (g) per deciliter (dL) of whole blood. Both the deficiency of Hb and excessive Hb cause disease. The normal ranges for Hb depend on the age and, beginning in adolescence, the gender of the person. The normal ranges are: Newborns: 17 to 22 g/dL, One (1) week of age: 15 to 20 g/dL, One (1) month of age: 11 to 15 g/dL, Children: 11 to 13 g/dL, Adult males: 14 to 18 g/dL, Adult women: 12 to 16 g/dL, Men after middle age: 12.4 to 14.9 g/dL, Women after middle age: 11.7 to 13.8 g/dL [2]. Two problems arise due to lack off sufficient amount of red blood cells (low Hb level) or excessive red blood cells (high Hb level): i) Anemia, ii) Polycythemia. According to World Health Organisation (WHO) anemia is a common disease and about 1.62 billion people all over the world suffered from anemia [3]. Every year, over 10 million people dies due to different diseases caused by anemia [4]. Therefore, regular measurement of blood Hb level is essential for the treatment of anemic patients [5] and premature babies [6], and dengue fever [7].

Glucose, is one of a group of carbohydrates known as simple sugars. The body produces glucose from foods that supply energy to all the cells in the body. But, if too much glucose remains in the blood it causes problems. Diabetes is one of the most chronic diseases in the world [8] caused when the body system cannot control sugar level in the blood. Diabetes is a serious health concern that has been proclaimed a worldwide epidemic by the World Health Organization (WHO) because of its quickly expanding rate. The current estimates by the International Diabetes Federation suggest that 415 million people have diabetes worldwide in 2015 and foresee it increasing to 640 million by 2040 [9]. In addition, patients with chronic diabetes are more likely to suffer from a variety of ailments, including heart disease, kidney damage, and lead to vision loss [10]. Every year, almost 4 million deaths are caused by high blood glucose [11]. Insulin produced by the pancreas lowers blood glucose. Absence

or insufficient production of insulin, or an inability of the body to properly use insulin causes diabetes. Diabetes is of two types: Type-1 is found in teenagers caused body does not produces enough insulin, Type-2 is found in adults caused when body produces insulin but can not use effectively. Former names for these conditions were insulin-dependent and non-insulin-dependent diabetes, or juvenile onset and adult-onset diabetes. Sometimes it is hard to detect the diabetes type, and further tests are required to identify the differences between diabetes Type-1 and Type-2 or more [12]. When the level of glucose is < 3.9 mmol/L, it is called hypoglycemia, and when the level of glucose is > 7.8 mmol/L, it is called hyperglycemia. If the level of blood sugar exceeds the typical range of 3.9 to 7.1 mmol/L or (70 to 130 mg/dL), it causes many long-term health issues [13]. Continuous monitoring of blood glucose level can help and prevent the level of hyperglycemia in diabetic patients. To reduce the risk of diabetes and heart disease, one must keep the level of blood sugar within a safe range [14]. Long term diabetes is very risky because it can increase the risk of stroke and other heart diseases, damage kidneys and nerves and lead to blindness [15]. Continuous monitoring of blood glucose level is very important for diabetes patients.

1.2 Hemoglobin and Glucose Measurement Techniques

Hemoglobin or glucose level estimation can be viewed as diagnosis process to measure the amount of hemoglobin or glucose exists in the blood. There are mainly three ways to measure the hemoglobin or glucose level: i) invasive technique, ii) minimally technique, and iii) non-invasive technique.

1.2.1 Invasive Technique

A medical procedure that invades (enters) the body, usually by cutting or puncturing the skin or by inserting instruments into the body. Various invasive methods are being used for blood component measurement. Most of these method measure blood components drawing blood via needle from the body (Figure 1.1). These methods are painful, inconvenient and costly for the patient due to frequent blood collection, and do not allow real-time monitoring [16, 17]. These procedures are often deleterious for children and people with needle-phobia. Needle phobia is the extreme fear of medical procedures involving injections or hypodermic needles affecting approximately 10% of the world population [18]. As needle is necessary for invasive measurement, people with needle-phobia seem to be unwilling to measure. However, the invasive technique is more precise and trustworthy, but it requires a well-resourced laboratory with skilled personnel, the majority of whom are inaccessible in a remote areas [19]. Moreover, with the repetitive use of needle to draw blood, finding veins gets harder to draw blood.

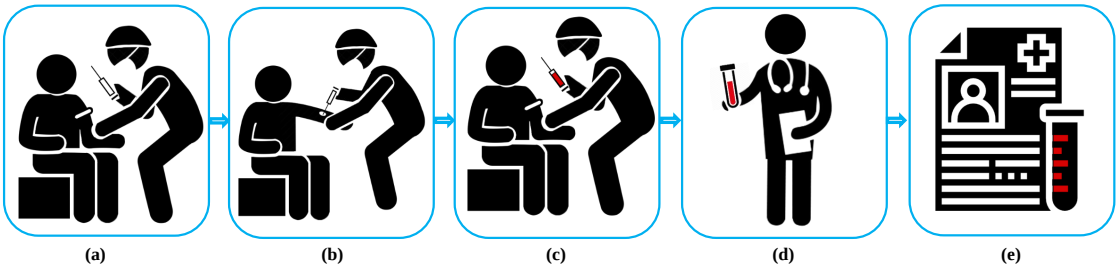

Figure 1.1: Invasive blood components level measurement process in clinical setup: (a) patient ready for blood test, (b) blood collected using needle, (c) venous blood obtained via venipuncture, (d) analysis the blood component in laboratory, and (e) laboratory measurement result.

1.2.2 Minimally Invasive Technique

These approaches rely either on the interaction of electromagnetic radiation with the tissue or the extraction of fluid across the barrier. The structure and physiology of the skin make the technical realization of transdermal hemoglobin monitoring a difficult challenge. The techniques involving transdermal fluid extraction circumvent and compromise the barrier function of skin's outermost and least permeable layer, the stratum corneum, by the application of physical energy [20].

1.2.3 Non-Invasive Technique

Non-invasive systems have mainly three functional units [21] shown in Figure 1.2. A data collection unit that acquires image or video data from the subject. A feature extraction unit that takes raw data and generates features from it. A measurement unit that estimates and validates results using different learning models (e.g machine learning model, and deep learning model, etc.). The non-invasive methods are more convenient to the patients as only bio-data (image, video etc.) is enough to measure the blood components instantly. Although invasive methods are more reliable, it is often costly and required well-equipped diagnostic center with properly trained personnel.

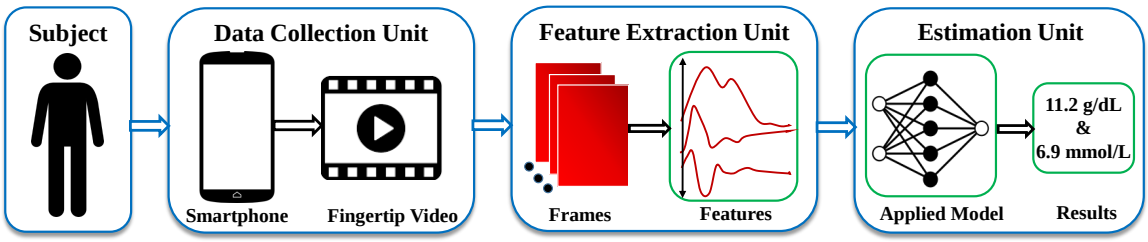

Figure 1.2: An overview of non-invasive blood component (Hb and Gl) measurement technique.

1.3 Motivation

Recently, photoplethysmogram (PPG) are widely used for vitals psychological parameters monitoring. PPG is an optical measuring technique used to measure volumetric changes in blood circulation [22]. PPG device comprises of a light source to illuminate tissue and a sensor to detect the reflected light. Numerous researchers have studied a variety of physiological parameters using the PPG signal due to its ease of use, low cost, and user-friendly setup [23]. For example, hemoglobin level estimation [24], heart rate monitoring [25], sleep monitoring [26], blood pressure estimation [27], and glucose level measurement [28]. PPG based near-infrared spectroscopy is most admired technique by the researchers because of its get-at-able and cheap setup [29]. Conventionally, PPG signals are acquired using optical techniques like sensor-based devices, chips, or pulse oximeters [27, 30, 31, 32]. Recently, several smartphones have built-in sensor systems for instantaneous measurement of heart rate, and oxygen saturation based on PPG signals. Patients who need constant health monitoring and health professionals can benefit from these non-invasive approaches [33]. However, technological improvements have enabled the smartphone camera to act as a sensor. For example, in the year 2015, Devadhasan et al. [34] used Samsung camera to estimate Gl. In the year 2016 and 2017, Wang et al. [35, 24] created an app using Nexus-5p and Nexus-6p called HemaApp to calculate Hb from fingertip video. In the same year, Anggraeni et al. [36] constructed a system using digital image of palpebral conjunctiva captured with an Asus Zenfone 2 Laser. In 2019, Hasan et al. [37] designed the SmartHeLP smartphone application utilizing Nexus-4p to determine the Hb level. In the year 2019, Chowdhury et al. [38] developed a non-invasive approach to estimate the Gl using the iPhone 7 plus. In the same year, Zhang et al. [39] developed a non-invasive blood glucose measurement system based on smartphone PPG signal.

Therefore, we are motivated to develop a non-invasive hemoglobin and glucose estimation method that aids doctors as well as patients to measure hemoglobin or glucose levels easily.

1.4 Problem Statement

The vast majority of blood component estimation technology commercially available is invasive or minimally invasive. Invasive devices for monitoring blood hemoglobin or glucose are poorly constructed and uncomfortable, whereas minimally invasive technologies have a limited lifespan and stability. Drawing blood from a vein involves the insertion of a needle associated with which patients may feel discomfort, pain, numbness, or a shocking sensation, and afterwards itching or burning at the collection site. These procedures are often traumatic for children and mentally disabled persons. Additionally, patients require travel to a medical facility which can be time-consuming and involve some expenses. Consequently, there is a need for a cost-effective, advantageous, non-invasive technology that can improve

routine blood testing. Existing blood component measurement techniques have the following limitations.

- Most of the commercially available devices for hemoglobin and glucose measurement are invasive or minimally invasive.
- There are some commercial non-invasive point-of-care tools for hemoglobin and glucose levels assessment. Most of these solutions suffer from one or more of the following limitations: 1) challenging data collection processes; 2) complex data analysis and feature extraction processes; 3) affordability and portability; and 4) lack of user-friendliness and costly external modules [40].
- Most of the existing techniques use specific hardware, e.g., laser light and finger chip, to acquire the PPG signal [41, 42].

1.5 Specific Objective

The main objective of the research is to develop a smartphone based non-invasive technique for blood components measurement (hemoglobin and glucose). To reach the goal the study will be carried out with the following specific objectives:

- Study the existing non-invasive methods for blood components measurement.
- Collect the fingertip video placing index finger on NIR-LED board through smartphone primary camera.
- Generate the PPG signal from the fingertip video and extract optimal PPG characteristic features from the generated PPG signal.
- Develop a non-invasive hemoglobin and glucose levels estimation method using deep neural network models.

1.6 Methodology

In this study, we have proposed a non-invasive method to estimate blood component (hemoglobin and glucose) levels with smartphone PPG signals extracted from fingertip videos and deep neural network model. The method has three basic steps. Initially, a near-infrared light-emitting diode (NIR-LED) kit/device is used to illuminate the finger and a smartphone to acquire a 15-second fingertip video. In the second step, frames are separated from each fingertip video. The red, green, and blue channels are separated from each frame, and the PPG signal is extracted from the channel with the highest intensity. Butterworth bandpass filter is applied to remove the high-frequency noise and motion artefacts. A peak detelction algorithm is used to select the best PPG cycle. Therefore, features are extracted from the preprocessed selected PPG cycle and its derivatives (PPG′ and PPG″), as well as the Fourier transform. After feature extraction, the maximal information coefficient (MIC) feature selection technique has been applied to select the optimal feature set and discard redundant and irrelevant features for hemoglobin or glucose measurement. Finally, in the last step

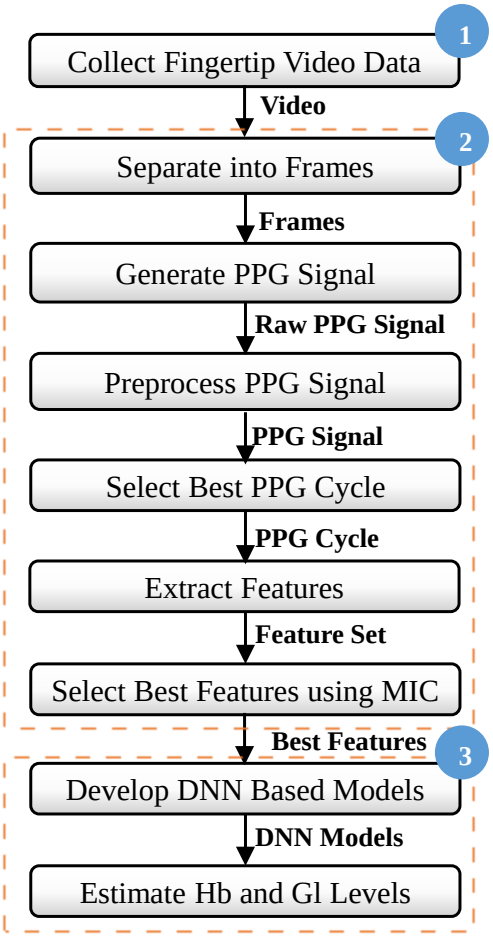

Figure 1.3: Block diagram of proposed method: step 1: data collection, step 2: feature extraction and seelction, step 3: model development and estimation.

two independent DNN based models have been developed using the optimal feature sets to estimate hemoglobin and glucose levels. Overall, functional block diagram of the proposed method is illustrated in Figure 1.3.

1.7 Scope of the Thesis

Recently, smartphone-based non-invasive techniques have been considered for various blood component levels assessment. In this study, a new non-invasive technique is proposed to estimate the hemoglobin and glucose levels using a smartphone PPG signal extracted from fingertip video. Overall the important scopes of this thesis are as follows:

- Data collection protocol can be improved using a smartphone camera that can capture a fingertip video under low-cost near-infrared (NIR) LED lights.
- Introducing novel video-image processing techniques to generate PPG features of fingertip video.
- Regression algorithms open opportunities for the development of estimation models, that can adapt to a new user's fingertip videos and, update the model from their PPG

features.
- The program is written in Python 3.6 version.

1.8 Contribution

Major contributions of this study are summarized below:
- Constructing a wearable data collection kit with NIR LEDs to collect fingertip videos.
- Generating the PPG signal from video data as well as selecting the best PPG cycle for feature extraction.
- Extracting features from preprocessed selected PPG cycle and its derivatives, and selecting the optimal feature set using MIC feature selection algorithm.
- Developing the deep neural network models to assess blood hemoglobin and glucose levels non-invasively.

1.9 Organization of the Thesis

The rest of this thesis is organized in five chapters, which are as follows:
Chapter II provides an overview of the existing works related to blood components measurements with their lacking and achievement. This chapter made the scope of our work. A summary of the literature survey is also provided in tabular format at the end of this chapter.
Chapter III explains theoretical consideration and machine learning algorithms.
Chapter IV explains our proposed methodology elaborately. From data collection to model development every steps of the proposed system is discussed here.
Chapter V describes experimental analysis and performance analysis of our work along with the comparison of results works.
Chapter VI ends with concluding remarks and future directions.

CHAPTER II

Literature Review

2.1 Introduction

The smartphone is a portable, affordable and convenient platform for developing point-of-care health tools. Non-invasive techniques are essential for patients who require to monitor blood tests regularly. There are numerous noninvasive hemoglobin or glucose measurement methods related to our work. In this chapter, we present a thorough survey of existing literature on hemoglobin or glucose estimation to compare and contrast with our proposed method. The shortcomings and achievements of their work are also identified. The chapter ends with a summary of the literature survey.

2.2 Invasive Method

Most extensively used technologies for measuring blood hemoglobin and glucose are invasive. The Medonic M-series M32 hematological analyzer is one such equipment. At first, 3-9 mL blood sample is collected from the patients and inserted into the machine, and it takes about one minute to produce results after analyzing the blood sample.

Another way of invasive hemoglobin level estimation was accomplished by an implantable optic sensor interface, which can measure, control, monitor, and report blood component levels continuously [43]. By using a thin, fork-shaped sensor with an electromagnetically sensitive array comprising optical sources and detectors, Sun et al. implanted the sensing system within subcutaneous tissue to continuously monitor the levels of blood components.

2.3 Minimal-Invasive Method

Blood components such as hemoglobin and glucose are measured using a minimally invasive technique that requires only a small volume of blood. Despite the blood draw, the minimally invasive method is simple, portable and inexpensive compared to the invasive method and can produce results quickly.

HemoCue® is a widely used minimally invasive device for measuring hemoglobin [44]. It requires a small blood sample for hemoglobin estimation within a minute. A drop of blood is collected in a cuvette and never tops off the cuvette after the initial filling. Clean any excess blood from the cuvette using a lint-free wipe. Inspect the cuvette for air bubbles. Place the cuvette in HemoCue® instrument. Gently push the holder into the photometer. Finally, the estimated hemoglobin level is shown on the screen after 15-45 seconds.

Figure 2.1: Conventional blood glucose measurement device.

Glucose meter is used to measure blood glucose [45]. A small drop of blood is obtained by pricking the skin with a lancet and is placed on the disabled strip. Strips are a consumable element containing chemicals that react with glucose in the drop of blood is used for each measurement. The strip is then inserted into the device, and reading the blood sample it calculate glucose level. Typically, it is able to show the result on the screen within 60 seconds (Figure 2.1).

2.4 Non-Invasive Method

Wang et al. [35] developed a smartphone-based application as HemaApp, using the smartphone camera and multiple lighting sources, including infrared LEDs that illuminate the patient's fingertip. A smartphone Nexus-5p was used for recording a series of videos with white, 880 nm, and 970 nm LED array. They focused on three different hardware embodiments, where the first embodiments included white flash + infrared emitter, the second one consisted of incandescent lamp + white flash + infrared emitter, and the final one was made white flash + series infrared LED array. A high-band pass filter was used to calculate average intensity for each channel. Then Fast Fourier Transform (FFT) and Support Vector Machine (SVM) regression were applied for each combination of datasets. However, this is not sufficient for the people whose Hb level below 8 g/dL (heavily anemic). The limitation of HemaApp is that they collected data by using a Nexus-5 device and only one brand of the intense light bulb. Results could be varied according to the different brand devices. They achieved a correlation (R) result between 0.69 and 0.82, and RMSE value between 1.26 and 1.56 g/dL. Edward et al. [24], improved the configuration of hardware for amplifying the weaker signal of Blue and Green. They estimated the blood Hb level without using an IR LEDs. In this case, they obtained Pearson correlation of 0.62 and an RMSE of 1.27. They

also compared their estimated Hb with Masimo Pronto. In addition, they found that the effect of ambient light in this study is significant.

Pai et al. in [46], developed a cloud computing-based glucose monitoring technique using near-infrared photoacoustic spectroscopy. A portable embedded system collected photoacoustic signals from tissue using FPGA, and the signal was denoised at a very high speed in the back-end. Multiple features of the photoacoustic signal were applied to a kernel-based regression algorithm to predict the glucose concentration in the blood. The mean absolute relative difference of the calibration algorithm was 9.64. Ramasahayam et al. in [41] constructed a PPG signal acquisition module based on the NIR spectroscopy technique for measuring Gl levels. The module consisted of the finger clip with LED (935 nm, 950 nm, and 1070 nm wavelengths) and a photodetector constituting an optode pair to detect the light intensity change. The acquired PPG signal was processed, and an artificial neural network model was implemented on field programmable gate array (FPGA) to predict blood glucose levels. The mean square error of estimation was 1.02 mg/dL. The above two methods require a specialized hardware toolkit for the collection of PPG signals. In addition, transmitting the acquired signals to the computer for further analysis is also time-consuming.

M. Anggraeni and A. Fatoni [36] introduced a non-invasive anemia detection system based on a digital image of palpebral conjunctiva captured by a smartphone camera. Digital image of the inferior palpebral conjunctiva was captured with an Asus Zenphone-2 Laser smartphone, ambient lighting without flash, and then color-corrected with white paper. The color intensity (R, G, B) was extracted from raw data using Colorgrab software (Loomatix), then evaluated using regression analysis. Among the three-color (R, G, B) intensity levels, red color intensity resulted in a high correlation with clinically measured Hb levels and gained $R^2 = 0.8139$.

Chowdhury et al. [38] developed a non-invasive approach to estimate the BGL based on smartphone video. A smartphone camera with 30 frames per second (fps) and 30 fps was used to record the fingertip video of 18 subjects and then convert it to the PPG signal. Gaussian filter along with Asymmetric Least Square methods was applied to reduce the noise of the PPG signal and then extract the features from it. Finally, the principal component regression algorithm was applied to estimate the glucose level, and the standard error of prediction (SEP) was 18.31 g/dL. In [47], same authors improved video data quality by using various smartphone cameras and sensors. Four regression methods were employed to measure the glucose level. The partial least square regression model performed better and achieved the lowest SEP at 17.02 g/dL. The signal acquisition was simple and portable, but the preprocessing was complicated, and models could not offer outperforming results.

In [39], the authors proposed a non-invasive blood glucose measurement system based on smartphone video data and a machine learning algorithm. A smartphone camera with 28 fps (sampling rate of 28 Hz) was used to collect 30–40 second long fingertip video data. Red, green, and blue channels were extracted from video frames and converted to PPG signals. 67

features were then extracted from the valid PPG signal and its derivatives. Finally, a subspace KNN classifier was applied to estimate the blood glucose level. The overall testing accuracy of the model was 86.2%.

Kavsaoğlu et al. [42] introduced a non-invasive method to predict blood hemoglobin levels using the characteristics of the PPG signals. In their study, a data acquisition card was used to receive PPG signals from 33 subjects without taking any blood samples. At the same time, blood count and Hb concentration were concurrently recorded using a device called "Hemocue Hb-201TM". Forty time-domain characteristics features were obtained from the original PPG signal as well as its 1st and 2nd derivatives. For the estimation of Hb level, eight different regression methods like Least Squares Regression (LSR), Generalized Linear Regression (GLR), etc. were used. Besides, Correlation-based Feature Selection (CFS) and RELIEF Feature Selection (RFS) techniques were applied to select the best feature set. Among eight regression methods, the support vector-based regression model was performed better compared to other models for prediction of Hb level.

In article [48], they developed a device called "Masimo Pronto" for screening (non-invasively) the anemia in infants. The "Masimo Pronto" is a non-invasive care testing device that can accurately measure the level of blood hemoglobin. They used the Masimo device to collect Hb data from 97-children, and they also took venous Hb levels. For assessing the accuracy and utility of the device, both invasive and non-invasive Hb levels were compared. A correlation coefficient of 0.47 was observed in the Masimo device with a sensitivity of 82% when the level of Hb was under 11.5 gm/dL. They also observed a negative predictive value of 95%, and in this situation, the Hb concentration was 11 gm/dL.

S. Haxha and J. Jhoja [49] reported a non-invasive glucose monitoring system based on image result for near-infrared spectroscopy to estimate the blood glucose levels. For this, NIR transmission spectroscopy was used, and tests were performed both in vitro and in vivo. To compare the performance of the proposed system, an invasive sensor, "TRUE result twist" was used. Experimental research has proved a correlation between the voltage of the sensor output and concentration of glucose, where the output voltage of the sensor increases as the concentration of glucose increases. The proposed prototype of the non-invasive NIR-based glucose sensor is considered as a low cost and showed a promising result in vitro. For estimating the accuracy of the technique, multiple linear regression was used here, and the R^2 term was equal to 0.96. But they faced some problems, as skin roughness and different body fluids could impact on the performance of the model.

Hasan et al. [37] developed SmartHeLP, a smartphone-based Hb level estimation technique using ANN and fingertip videos. The authors collected 10-second (300 frames) fingertip video each from 75 participants of 20-56 year of ages and the levels of Hb were from 7.6 to 13.5 gm/dL. Red, Green, and Blue pixel intensities from each frame were separated for feature extraction, and the ANN-based model was developed using these features to predict the Hb level. They observed a correlation of R^2 0.93. To reduce the necessary feature space,

Table 2.1: Summary of several non-invasive techniques used for blood component levels measurement (Hemoglobin, and Glucose).

Author(s)	Purpose	Device	#Sub	Signal	Algorithm(s)	Performance
Al-Baradie and Bose [50]	Hb	HemoCue	10	PPG	–	$PMRE = 0.56\%$
Wang et al. [35]	Hb	Nexus-5p	31	PPG	SVR	$R = 0.82$
Edward et al. [24]	Hb	Nexus-6p	32	PPG	LR	$R = 0.62$
Pai et al. [16]	Gl	FPGA	24	Spectra	KBR	$RMSEP = 9.64$
Ramasahayam et al. [41]	Gl	FPGA	50	PPG	ANN	$RMSE = 5.84$
Anggraeni and Fatoni [36]	Hb	Asus Zen-Fone 2 Laser	20	-	LR	$R^2 = 0.81$
Chowdhury et al. [38]	Gl	iPhone 7 Plus	18	PPG	PCR	$SEP = 18.31$
Zhang et al. [39]	Gl	iPhone 6s Plus	14	PPG	KNN	$Acc = 86.2$
Kavsaoğlu et al. [42]	Hb	Hemocue Hb-201TM	33	PPG	CART, LSR, GLR, MVLR, PLSR, GRNN, MLP, and SVR	$R^2 = 0.92$
Hsu et al. [48]	Hb	Masimo Pronto SpHb	97	–	Pronto SpHb	$R = 0.47, p - value < 0.001$
S. Haxha and J. Jhoja [49]	Gl	TRUEresult twist	5	Spectra	MLP, LSR	$R^2 = 0.96$
Hasan et al. [37]	Hb	Nexus-4p	75	PPG	ANN	$R^2 = 0.93$
Glovanni et al. [51]	Hb	iPhone 4s, Huawei p7	113	–	KNN	$R = 0.65$
Dimauro et al. [52]	Hb	Smartphone	102	–	KNN	$Acc = 0.982$

* Hb = Hemoglobin, Gl = Glucose, #Sub = Number of participant, SVR = Support Vector Regression, LR = Linear Regression, FPGA = Field-programmable Gate Array, KBR = Kernel-based Regression, CART = Classification and Regression Trees, LSR = Least Square Regression, GLR = Generalized Linear Regression, MVLR = Multivariate Linear Regression, PLSR = Partial Least Squares Regression, GRNN = Generalized Regression Neural Network, MLP = Multilayer Perceptron, KNN = K-Nearest Neighbour, *Acc* = Accuracy.

they identified a specific Region of Interest (ROI) in the image frame.

In [51], the authors designed a non-invasive system to detect the anemia using conjunctiva image. Two smartphones, iPhone 4s and Huawei p7, were used to collect the conjunctiva images. They collected data from 113 subjects both anemic and healthy, and K-nearest neighbour classifier with 10-fold cross-validation used to determine the risk of anemia. They

obtained a correlation coefficient results between 0.52 and 0.65.

2.5 Discussion

Table 2.1 represents several existing methods to estimate the different blood components, such as hemoglobin, and glucose. Considering the existing literature, we observed that digital image or video data of eye conjunctiva [36, 51] and fingertip [24, 35, 37, 38, 39] can measure different blood components such hemoglobin, and glucose. It also shows that the PPG signal contains potential information regarding different blood components. Though, there are a lot of research has been done for the measurement of hemoglobin and glucose, but only a few researches have been used smartphone camera for collecting data. Most of the existing techniques use specific hardware, e.g., laser light and finger chip, to acquire the PPG signal [41, 42] or spectra analysis [16, 49]. To sum up, there is up to now no non-invasive method for measuring blood component levels based on PPG signal from a fingertip video, which has the advantages of time efficiency and no calibration requirement. Therefore, we propose a method to estimate hemoglobin and glucose using the smartphone video and deep neural network models.

CHAPTER III

Theoretical Aspects

3.1 Introduction

For non-invasive measurement, optical properties of living tissue have been used for the calculation of the difference in absorbance properties of blood constituents. The absorbance properties can be measured in transmissive and reflective mode where various wavelengths of light can travel through living tissues. In this chapter, we describe the modified beer-lambert law, basic concept of photoplethysmogram (PPG) and different learning algorithms for hemoglobin and glucose levels estimation.

3.2 Theoretical Foundations

3.2.1 Beer-Lambert law

Light absorbance can be measured by detecting changes in the transmitted and reflected light. The changes in transmitted and reflected light mainly depends on structure, volume, medium, thickness, refractive index of hemoglobin, absorption properties of blood and tissue [53]. According to Beer-Lambert law, the absorption of light is proportional to the concentration of a medium and the path length, given by:

$$I_m = I_o e^{-\alpha CL} \tag{3.1}$$

where, I_m is the measured light intensity, I_o is the incident light intensity, α is the light absorption coefficient, C is the concentration of a blood component, and L is the light path length. In our case, the finger has three different absorption's for a wavelength of light (λ) due to Hemoglobin (Hb), plasma (P), and tissue (T). So, the light absorption (under the light wavelength λ) by a finger is:

$$I_{m,\lambda} = I_o e^{-L(\alpha_{tissue,\lambda}[T]+\alpha_{hemoglobin,\lambda}[Hb]+\alpha_{plasma,\lambda}[P])} \tag{3.2}$$

The variation in arterial thickness ΔL affects only the path length of hemoglobin and plasma. The effect of tissue can be eliminated by measuring the ration of maximum and minimum light intensity, given by:

$$\frac{I_{H,\lambda}}{I_L,\lambda} = e^{\Delta L(\alpha_{hemoglobin,\lambda}[Hb]+\alpha_{plasma,\lambda}[P])} \tag{3.3}$$

Taking the log of both sides of the equation, we can write:

$$\ln \frac{I_{H,\lambda}}{I_L,\lambda} = \Delta L(\alpha_{hemoglobin,\lambda}[Hb] + \alpha_{plasma,\lambda}[P]) \tag{3.4}$$

Finally, the absorption of the blood in each wavelength can be computed by (3.4).

3.2.2 Photoplethysmography

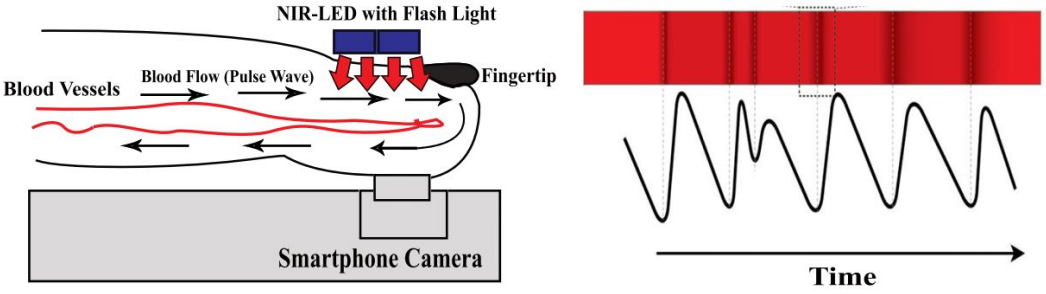

Figure 3.1: Photoplethysmography (PPG) principle by smartphone. PPG signal generated from volumetric blood flow changes via light passing through the fingertip, transmitting off of the tissue, and then passing to the smartphone camera's image sensor.

Photoplethysmography (PPG) is an optical measuring technique used to measure volumetric changes in blood circulation [54]. Recently, PPG signals are widely used for vitals psychological parameters monitoring. PPG systems are considered to be a low cost, convenient, and user-friendly which can be easily obtained by surface-sensing method with

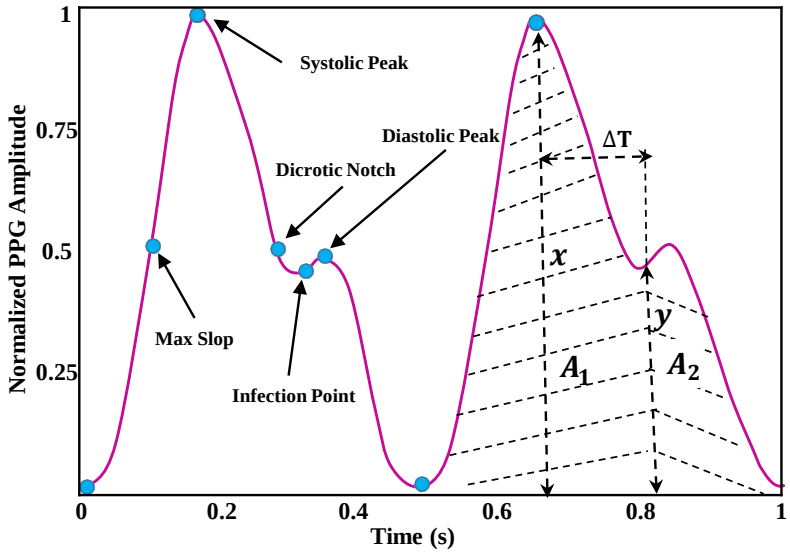

Figure 3.2: A typical two pulse PPG signal with its characteristic points. Here, x, y portrait the amplitudes of systolic and diastolic peaks, respectively, and ΔT is the time period between these two points. A_1/A_2 is the ratio of inflection.

minimal contact or cameras with imaging techniques [55]. Conventionl PPG device generally comprises of a narrow wavelength light source (ie, light-emitting diodes [LEDs] with certain colors such as infrared, red, or green) for illuminating the tissue and a a specific photodetector to sense the reflected light through the skin [42]. Periodic variations in the amount of light absorbed occur with blood volume, which can be utilized to obtain the PPG signal. Now, numerous smartphone cameras have integrated sensors to assess the physiological parameters based on the PPG signal. Smartphone camera in combination with the NID-LED is able to detect these small variations in color caused by the blood flow. The camera uses wide-bandwidth pixel-enabling color detection in the red, green, and blue range (RGB-color). Figure 3.1 illutrates the generation of PPG signal due to the volumetric changes in blood captured by smartphone camera. PPG is of either transmittance or reflectance type. In the transmittance type, LED used as the light source is placed opposite to photo detector while LED and photo detector are on same side in the reflectance type PPG. Figure 3.1 shows transmittance type PPG, where LED and smartphone camera are on opposite side of the finger. PPG has been applied in various clinical application, including heart rate monitoring [25], anemia detection [42], heart-rate validation [30], blood pressure estimation [27] and blood glucose level [31]. A typical two-pulse PPG signal with its characteristic points is depicted in Figure 3.2.

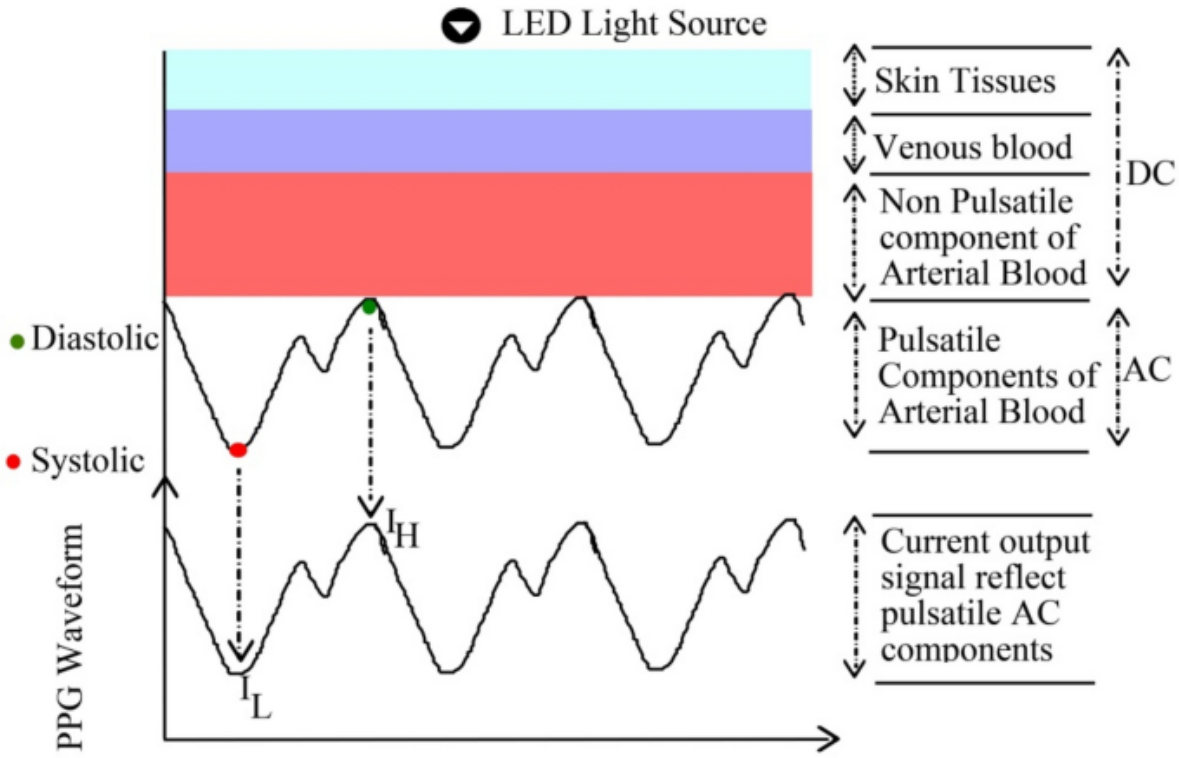

Figure 3.3: Light absorption in living tissue and variation due to blood volume [1].

Photoplethysmogram (PPG) is a signal which is optically obtained through a plethysmograph used for detecting the volumetric variation through blood circulation [29, 22]. When

light from LED is incident on living tissue, tissues and arteries mainly absorb it. Figure 3.3 shows light absorption from light source (LED) to receiver smartphone camera and resultant PPG waveform which represents a quasiperiodic signal. The waveform mainly consists of direct current (DC) component and alternating current (AC) component. First, the DC portion is generated by the optical signals reflected or emitted from tissues and the average blood volume of both arterial and venous blood, as presented in Figure 3.3. These components are almost steady since the DC component does not change much with respiration. The second part, the AC portion refers to differences in the blood volume of the cardiac beat synchronization received from the blood vessels. Following cardiac blood circulation methodology, the amount of blood in the arteries increases after the systolic period. On the other side of the coin, the arteries shrink during the diastolic period, and the amount of blood in arteries decreases. As a result, the intensity of the light received from tissues decreases at the time of systole, and the light transmitted from tissues increases during diastole. In arterial blood, the dynamic part of the signal is defined as AC signal and the static part is mentioned as a DC signal, as shown in Figure 3.3. The change in light intensity per unit time is known as the PPG signal.

3.3 Machine Learning Algorithms

A machine learning algorithm trains a machine to learn and apply acquired knowledge in predictions. Most of the current hemoglobin and glucose estiamtion models use machine learning algorithms. Here, we present a list of machine learning algorithms that we have used as reference models to assess Hb and Gl levels non-invasively. Finally, we have developed two seperate deep neural netwroks models for the estimation of Hb and Gl levels. Following sections are the descriptions of estimators that we have used in our study as the models.

3.3.1 Linear Regression

Linear regression (LR) is one of the simplest and popular technique for data analysis. It has tremendous use in biomedical field. The theorem behind every linear model is following [56]:

$$\hat{y}(w,x) = w_0 + w_1x_1 + w_2x_2 + ... + w_nx_n \tag{3.5}$$

where, w_0 = intercept, $w = w_1, w_2, ..., w_n$ are coefficients and $\hat{y}$ = predicted value. The optimization or loss function that we have to minimize is following:

$$min_w||Xw - y||_2^2 \tag{3.6}$$

3.3.2 Support Vector Regression

In support vector regression (SVR), the dataset are considered in high dimensional feature space. It finds out the maximum margin in case classification using support vectors which

can be called critical points of the dataset. Given a set of training samples as $D = \{x_i, y_i\}_{i=1}^{m}$ where, $x_i \in \mathbb{R}$ and $y_i \in Y$. In $\varepsilon - SVR$ [57], the aim is to find a function $f(x)$ with the most ε deviation from the actual y_i for all training data and at the same time as flat as possible. The relation between the input x_i and output y_i can be mapped using the regression function (3.7 and 3.8):

$$f(x_i) = \hat{y}_i = w_1 x_1 + w_2 x_2 + \cdots + w_m x_m + b \tag{3.7}$$

$$f(x_i) = w^T x, \qquad where \;\; w \in X, \;\; b \in \mathbb{R} \tag{3.8}$$

Flatness in (3.7) means small w; therefore, the norm, $||w||^2$ must be minimized. Formally, this problem can be written as a convex optimization problem [58]:

$$\begin{aligned} &minimize \;\; \frac{1}{2}||w||^2 \\ subject \;\; to \;\; &\begin{cases} y_i - w^T x_i - b \le \varepsilon \\ w^T x_i - b + y_i \le \varepsilon \end{cases} \end{aligned} \tag{3.9}$$

where, the constraints are infeasible, called the soft margin formulation [59], we can introduce the slack variables (ξ_i, ξ_i^*) and the formulation becomes,

$$\begin{aligned} &minimize \;\; \frac{1}{2}||w||^2 + C\sum_{i=1}^{m} \xi_i + \xi_i^* \\ subject \;\; to \;\; &\begin{cases} y_i - w^T x_i - b \le \varepsilon + \xi_i \\ w^T x_i - b + y_i \le \varepsilon + \xi_i^* \\ \xi_i, \xi_i^* \ge 0 \end{cases} \end{aligned} \tag{3.10}$$

In (3.10), the constant $C > 0$, controls the penalty amount deviations larger than ε. The ε-intensive loss function $|\xi|_\varepsilon$ described by

$$|\xi|_\varepsilon = \begin{cases} 0 & if \;\; \varepsilon|\xi| \le \varepsilon \\ |\xi| - \varepsilon & otherwise \end{cases} \tag{3.11}$$

According to the Lagrange multiplier and Karush–Kuhn–Tucker conditions, the dual form is transformed into an optimization function [60].

$$\min_{\alpha,\alpha^*} \frac{1}{2}\sum_{i=1}^{m}\sum_{j=1}^{m} K(x_i,x_j)(\alpha_i-\alpha_i^*)(\alpha_j-\alpha_j^*)+\varepsilon\sum_{i=1}^{m}(\alpha_i+\alpha_i^*)-\sum_{i=1}^{m} y_i(\alpha_i+\alpha_i^*)$$
$$s.t. \quad 0 \le \alpha_i, \alpha_i^* \le C \qquad i = 1,\ldots,m \tag{3.12}$$
$$\sum_{i=1}^{m}(\alpha_i-\alpha_i^*) = 0$$

The kernel functions transform the data into a higher dimensional feature space to perform the linear separation. $\varphi(x_i)$ mapped the data into a higher dimensional feature space [58]. The standard SVR to solve the approximation problem is

$$f(x_i) = \sum_{i=1}^{N}(\alpha_i-\alpha_i^*)K(x_i,x)+b \tag{3.13}$$

where, α_i, α_i^* are Lagrange multipliers. The kernel function $K(x_i,x)$ can be defined as linear dot product of the nonlinear mapping, e.g.,

$$K(x_i,x) = \varphi(x_i)\varphi(x) \tag{3.14}$$

From the above discussion, the SVR quality is affected by the penalty parameter C, the non-sensitive loss ε, the kernel function, and the parameters of the kernel. The radius basis function (RBF) kernel function is used in this experiment as follows:

$$K(x_i,x_j) = \exp\left(-\gamma||x_i-x_j||^2\right) \tag{3.15}$$

where, γ is width parameter of RBF kernel [61].

3.3.3 Artificial Neural Network

A the initial stage, a gradient descent backpropagation neural network was used in this study. It comprises of three layers: input layer, hidden layer, and output layer. Figure 3.4 illustrates the structure of our proposed ANN model. There are 36 features used to feed the ANN model in the input layer. In the hidden layer, there are 73 neurons with the ReLU activation function, while in the output layer, there is just one neuron with a linear activation function. The total number of nodes in the hidden layer determines as in (3.16).

$$L = (2n+1) \tag{3.16}$$

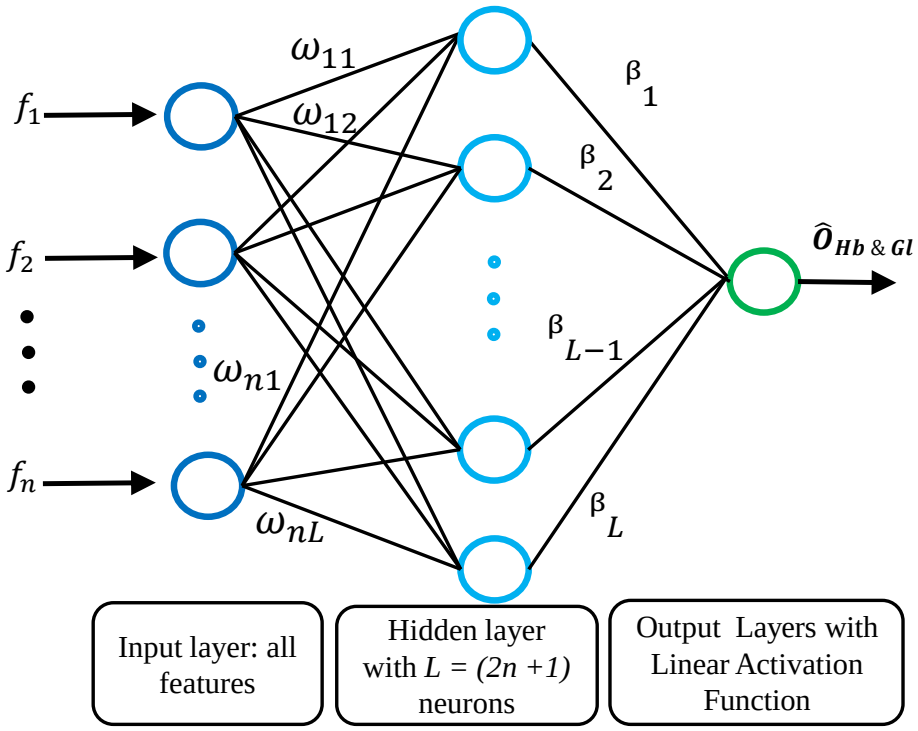

Figure 3.4: The architecture of proposed ANN models for Hb and Gl levels estimation.

where L is the number of hidden nodes and n is the number of input nodes. The output of each node in hidden layer is calculated using the (3.17).

$$\upsilon_j = \sum_i \omega_{ij} o_j + \beta_j \tag{3.17}$$

where ω_{ij} are the weights of each nodes and β_j is the bias. The hidden layer will change the input using the ReLU activation function as in (3.18).

$$o_j = \max(0, \upsilon_j) \tag{3.18}$$

Finally, at the output layer, a linear activation function is applied. The ANN model was trained on 100 epoch and 32 batch size. In order to ensure the model's validation, a 10-fold cross-validation procedure was used.

3.3.4 Deep Neural Network

Deep neural network (DNN) is a feed-forward, artificial neural networks comprising an input layer, several hidden layers, and an output layer. It is equipped with biases, weights, and activation functions such as a rectified linear unit (ReLU) [62]. The input layer consists of neurons equal to the number of features in the dataset, and the output layer is composed of a single neuron [63]. In this work, we explored a multilayer feed-forward network, where nodes of each layer receive the inputs from the previous layer. The output of nodes in one

layer will be the input of the next layer. The architecture of our proposed DNN model is shown in Figure 3.5. As shown in Figure 3.5, two neurons make up the output layer, while the input layer has as many neurons as the number of features. There are a total of four hidden layers: the first has 150 neurons, the second has 200 neurons and a dropout unit of 0.25, the third has 250 neurons, and the fourth has 300 neurons and a dropout unit of 0.5. The dropout method is an alternative and more efficient option for addressing DNN overfitting [64]. Suppose H hidden layers of neural network. Let $h \in \{1, 2, \cdots, H\}$ index of the hidden layers of the network. Let $f^{(h)}$ specify the inputs vector for layer h. At layer h, $\omega^{(h)}$ and $\beta^{(h)}$ are the weights and biases, respectively. Each neuron's hidden layer output can be expressed as in (3.19).

$$\upsilon_j^{(h+1)} = \sum_j \omega_j^{(h)} f^{(h)} + \beta_j^{(h)} \tag{3.19}$$

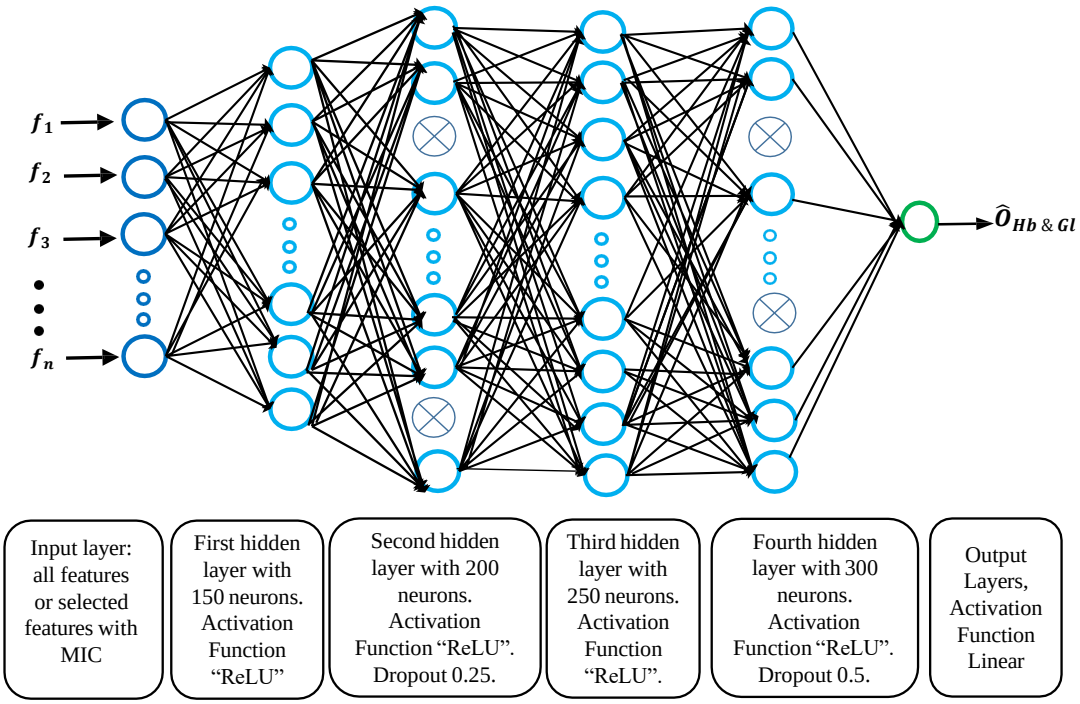

Figure 3.5: The proposed architecture of DNN model for Hb and Gl levels measurement.

Using the learning rate λ, the following equation is used to iteratively update the weight and bias vector [65].

$$(\omega^{h+1}, \beta^{(h+1)}) = (\omega^h, \beta^{(h)}) - \lambda \frac{\partial E_{Loss}}{\partial (\omega^h, \beta^{(h)})} \tag{3.20}$$

Using the ReLU activation function, the hidden layer neuron will modify the input above as in (3.21).

$$\varphi_{re}(\upsilon) = \max(0, \upsilon) \tag{3.21}$$

Finally, at the output layer, a linear activation function is employed.

$$\varphi_{li} = \upsilon' \tag{3.22}$$

where $\upsilon' = (-\infty, +\infty)$. Thus, the dense layer returns the sum of the activation function.

3.4 Conclusion

Photoplethysmography is an optically obtained plethysmogram that can be used to detect blood volume changes. In this chapter, we have presented how the smartphone camera, combined with the NID-LED, can detect these small variations in colour caused by blood flow. We have also described the various machine learning algorithms and deep neural network models. The detail of the proposed method from data collection to models development is presented in the next chapter.

CHAPTER IV

Proposed Method for Blood Component Estimation

4.1 Introduction

In this chapter, our proposed methodology is explained. The collection of fingertip video from the human subjects using a smartphone, generation of the PPG signal, selection of best PPG cycle, extraction of features from PPG signal, selection of optimal feature set using maximal information coefficien technique, and construction of DNN based model are briefly described throughout the chapter. The overall architecture of our proposed system are depicted in Figure 4.1.

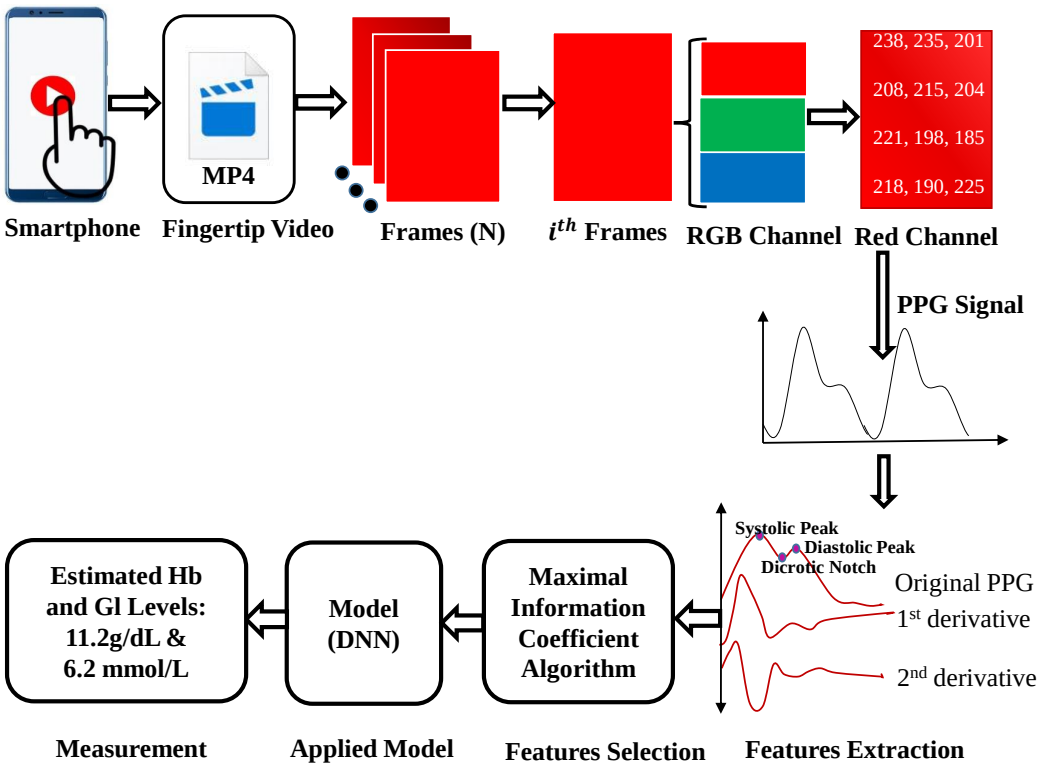

Figure 4.1: Overall functional block diagram of the proposed method.

4.2 Hardware Configuration

The proposed hemoglobin and glucose measurement system needs a data collection kit to illuminate the finger and a smartphone to collect the video. Conventionally, PPG signals are

acquired using optical techniques like sensor-based device or chip. In these cases, visible or NIR-LED are used for illuminating the finger or different parts of body tissues and a photodetector for measuring the amount of light either transmitted or reflected. Therefore, we aim to obtain PPG signals through the use of the smartphone camera to capture fingertip video and then analyzing the variation of light intensity reflected from a finger caused by the change of blood volume in systolic and diastolic cycles. Although some new smartphones are starting to be equipped with sensor or IR LEDs, the most smartphone have only white LED and do not have sensors for detecting the reflected/transmitted light. External lights, near-infrared lights, are required when a smartphone has no support to sense blood components non-invasively in living tissues. For fingertip-based data collection, we pointed out that a covered external NIR light source can provide the best PPG signal from a smartphone video. But the selection of near-infrared wavelength is the first step of hardware design and a critical issue to acquire the strong and clean PPG signal because we have to take wavelength as consideration for the absorption of light by blood, muscle, and skin tissues. From the study of several previously existing techniques, it is observed that most of the works used $475 - 2500$ nm wavelength light for acquiring the PPG signal. For example, Ramasahayam et al. [41] used 935 nm, 950 nm, and 1070 nm NIR-LED to acquire the PPG signal for estimating Gl level. In HemaApp [24], 880 nm and 970 nm, as well as 500-700 nm and 1300 nm NIR-LED, were used to measure the blood Hb concentration in two different studies. Al-Baradie and Bose [50] developed a LED-based Hb sensor system for acquiring the PPG signals at the wavelengths of 670 nm and 810 nm. Light absorbed of NIR wavelength range from $700 - 2500$ nm by tissues [23] is considerable to get the strong PPG signal as well as it can penetrate through the tissues of the finger between $1 - 2$ cm effectively [66]. In the NIR region, light absorption is lower than the other spectral areas for oxy-hemoglobin and

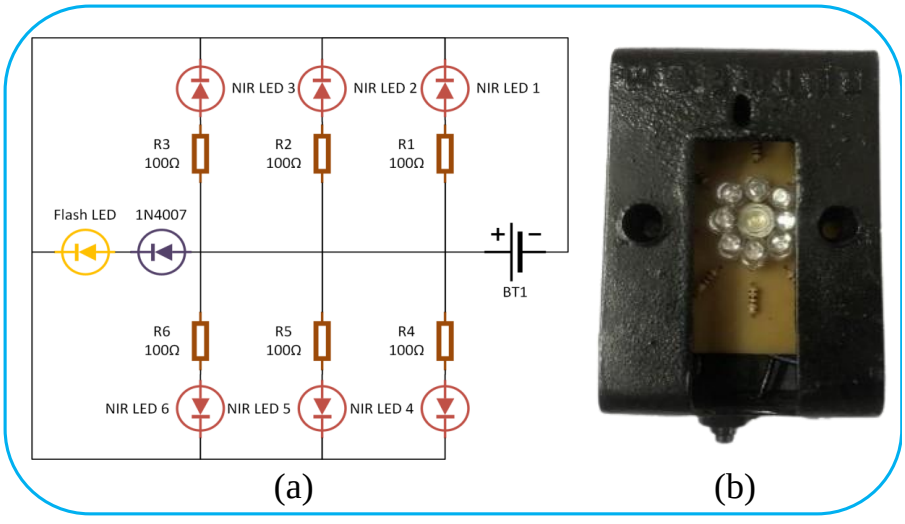

Figure 4.2: Illustration of external data collection kit: (a) Circuit diagram (b) External wearable device

deoxy-hemoglobin. Considering availability and financial restraints, it is easiest to get the near-infrared LED with 850 nm wavelength for our purpose. The data collection kit consists of circle with eight NIR-LED, and a white LED in the centre, as shown in Figure 4.2 (b). The function of the white LED is to amplify the intensity of NIR-LED. The external surface of the device is made to black so that the reflectance factor can hardly affect the analysis. Figure 4.2 illustrates the prototype of the data collection kit.

4.3 Video Data Collection

A 15 second long video of the right index finger was recorded using a smartphone's primary camera (Nexus-6p, 30 fps), while the finger was illuminated using the data collection kit. Simultaneously, the gold standard blood hemoglobin and glucose of these subjects were also collected using the clinical method. These two procedures were performed consecutively but separately (with an interval of less than one minute). Therefore, the blood component levels didn't change quickly. The reference standard value for hemoglobin was determined using the Sysmex XS-800i hematocrit analyzer, and the glucose value was measured with Thermo Scientific Konelab 60i, respectively, in the clinical laboratory. The authorities and medical teams of the Medical Centre Hospital, 953, O.R. Nizam Road, Chattogram, Bangladesh, approved the study. The blood sample of each subject for clinical measurement was collected just before taking the fingertip video. In the whole procedure, 93 subjects (59 males and 34 females; age: 32.67 ± 16.53 years) participated. The age and gender of the subject were also collected during the data collection process. The statistical information of the data collection is shown in Table 4.1. More details about the dataset is preseneted in Appendix Table A.1.

Table 4.1: Statistical inforamtion of clinical laboratory data.

Physical Index	Statistical Data
Age (years)	0 to 79 ($\mu = 32.81, \sigma = 16.57$)
Gender	59 male (63.5%); 34 female (36.5%)
Hemoglobin (g/dL)	7.9 to 21.49 ($\mu = 12.933, \sigma = 2.137$)
Glucose (mmol/L)	3.33 to 21.11 ($\mu = 6.64, \sigma = 2.97$)

* μ = mean, σ = standard deviation

Data collection is one of the vital stages of conducting research. Data can be corrupted within a moment for a simple mistake and affect all the next processes. The following guidelines were followed while recording the fingertip video.

- The subject's right fingers were clean and dry before capturing the fingertip video.
- The index finger was preferred, but other fingers were used according to the condition of the tissue if the index finger was injured.
- The fingertip video was recorded after taking clinical blood sample.

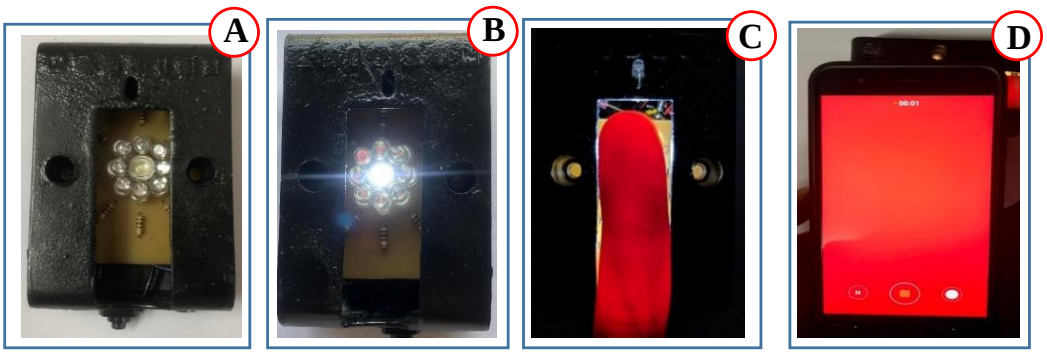

Figure 4.3: Fingertip video data collection kit/device: (A) NIR-LED device with power off, (B) NIR-LED device in turned on condition, (C) Index finger on the device while turned on, and (b) Video recorded with a Nexus-6p smartphone.

- External wearable device was constructed in a user-friendly manner so that participants can easily place the finger on the device.
- Same conditions (room temperature and light) were maintained during the acquisition of data from any participant.

After reviewing all the facts, the index finger was placed in the data collection kit during the recording period, as shown in Figure 4.3 (C), and the fingertip video was captured while the finger was illuminated, as shown in Figure 4.3 (D). Finally, a 15 second video was captured, placing a smartphone primary camera on the finger, according to Figure 4.3. The first 3 second and the last 2 second are discarded from each fingertip video to avoid unstable frames.

4.4 Generation of PPG Signal and Preprocessing

Photoplethysmogram (PPG) is a signal which is optically obtained through a plethysmograph used for detecting the volumetric variation through blood circulation [29, 22]. It reflects the movement of blood from the heart to the fingertip. According to heart blood circulation patterns, arteries carry more blood in the systolic period than the diastolic period. As a result, absorber (blood) of light in the tissue with arteries varies with these two blood circulation period. During the systolic period, the diameter of arteries is higher than the diastolic period and light passes through a longer path. In contrast, light passes a shorter path during the diastolic period. For these reasons, the light intensity is changed with time and the pattern is called PPG-wave. For generating the clean and good PPG signal from the image frame, the selection of optimal Region of Interest (ROI) is indispensable [67, 68]. To identify the ROI, HemaApp [35] used a centre segment of the frame of an image and calculated the average intensity for each channel of the centre segment of that image, Scully et al. [69] picked 50×50 array of pixels on the green channel and Jonathan et al. [70] extracted 10×10 block of the mean intensity value of the pixels from the central region. SmartHeLP [37] separated

a 10×10 pixels block from the image frame for identifying the best generated PPG signal's most adequate position. In this study, the average intensity for each channel is calculated by cropping image frame of 500×500 pixels from right to left section of the image. This is done because the image from this section is the most consistent and stable when the video of the fingertip is captured with the smartphone. Frame separation and cropping 500x500 pixels from each frame are graphically illustrated in Figure 4.4.

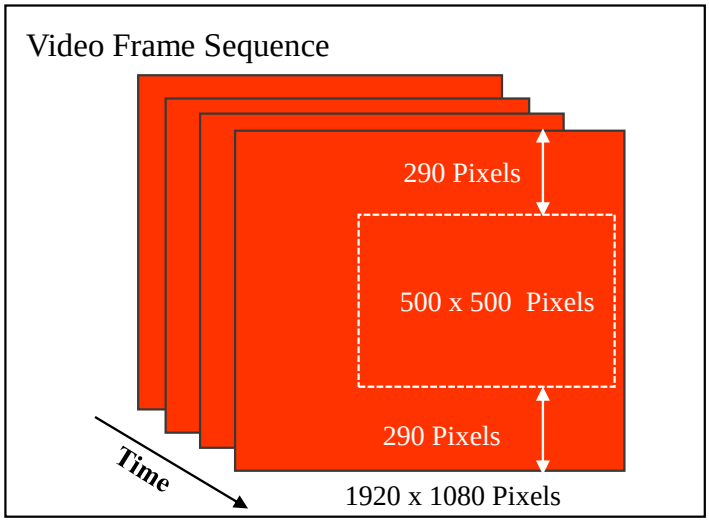

Figure 4.4: Frame separation and cropping ROI. Crop 500×500 pixels from the middle of right side from each frame.

As the PPG signal reflects the movement of blood from the heart to the fingertip, the characteristics of the PPG signal can provide information on the levels of blood constituent [71, 42]. Therefore, it is necessary to identify appropriate preprocessing and feature extraction methods to analyze the PPG signal precisely [72]. Blood's absorption of light is related to the variation in finger blood volume, which is reflected and captured in the video. Consequently, the same region's pixel intensity in successive frames is different. The most commonly applied method for obtaining the PPG signal from a recorded video sequence is calculating the mean brightness of a particular color channel in each frame, leading to the desired signal. Subsequently, the raw signal is processed with the objective of extracting the meaningful variations in intensity caused by the periodic propagation of blood pulse waves through the arteries [73]. A video data comprises a series of digital images called frames. A 15-second (30 fps) video is a series of 350 frames. The first 3 seconds (frame number 1 to 90) and the last 2 (frame number 291 to 350) seconds of each video are discarded due to unstable frames. The red $(225 - 245)$, green $(0 - 3)$ and blue $(15 - 25)$ channels are extracted from individual frame of the video. The intensity of the red channel is the highest among the three channels. Therefore, other channels are discarded. The continuous PPG signal is calculated

by overall pixel intensity variations in each frame. In this study, the PPG value of the i^{th} frame is calcuated in two ways.

- In the first step, for each video frame, the PPG value of the i^{th} frame is measured by (4.1) as the mean of the pixels. The PPG signal is acquired by plotting the computed mean of pixels from frames as shown in Figure 4.5.

$$PPG[i] = \frac{1}{total\_pixels} \sum_{i=1}^{total\_pixels} intensity_i \tag{4.1}$$

- In the second step, an adaptive threshold is defined as sum of half the minimum brightness and maximum brightness of i^{th} frame. The threshold value is selected empirically. This threshold is used to reject erroneous frames, i.e., frames that are too dark due to incorrect placement of the finger on the camera and NID-LED. Therefore,

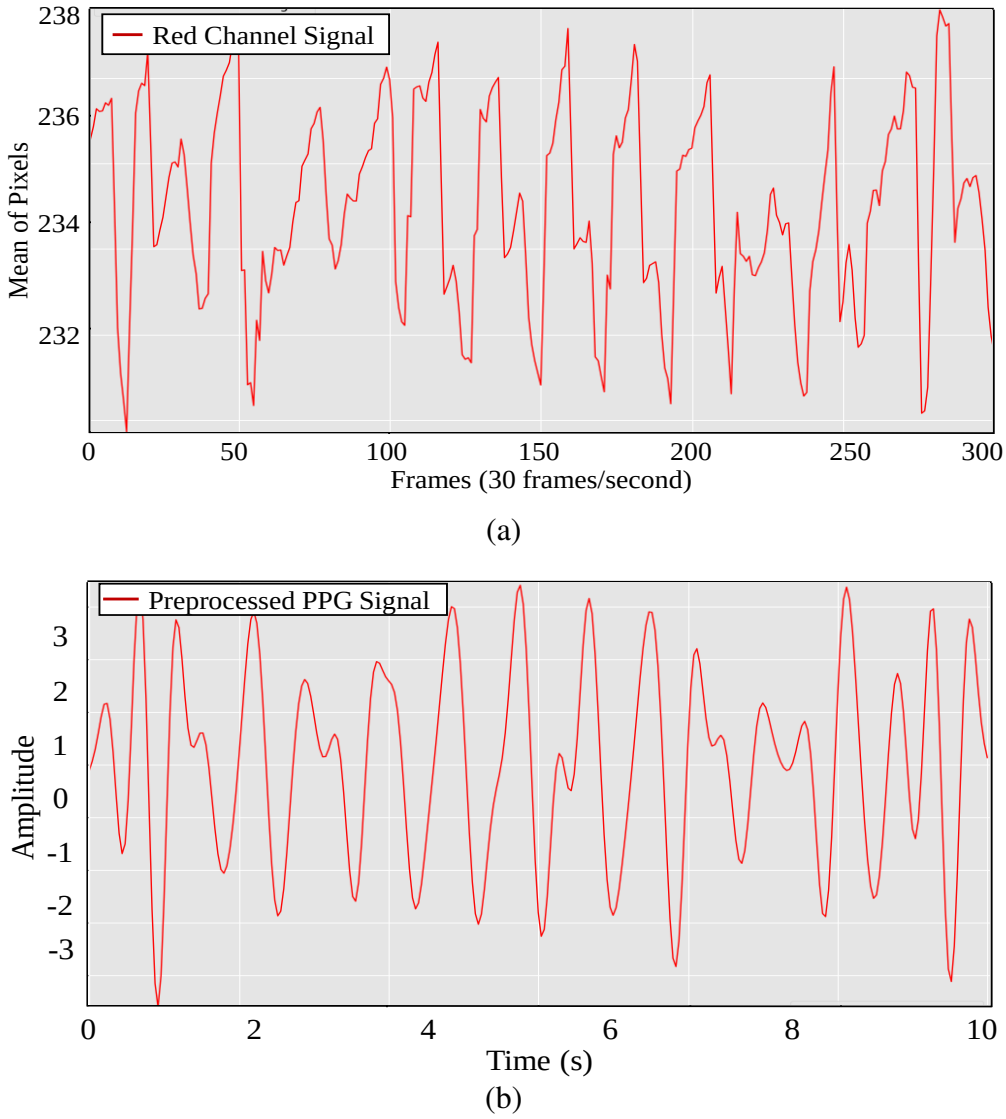

Figure 4.5: Generation of PPG signal from fingertip video using the mean of pixels of each frame: (a) raw PPG signal from fingertip video, (b) filtered PPG signal.

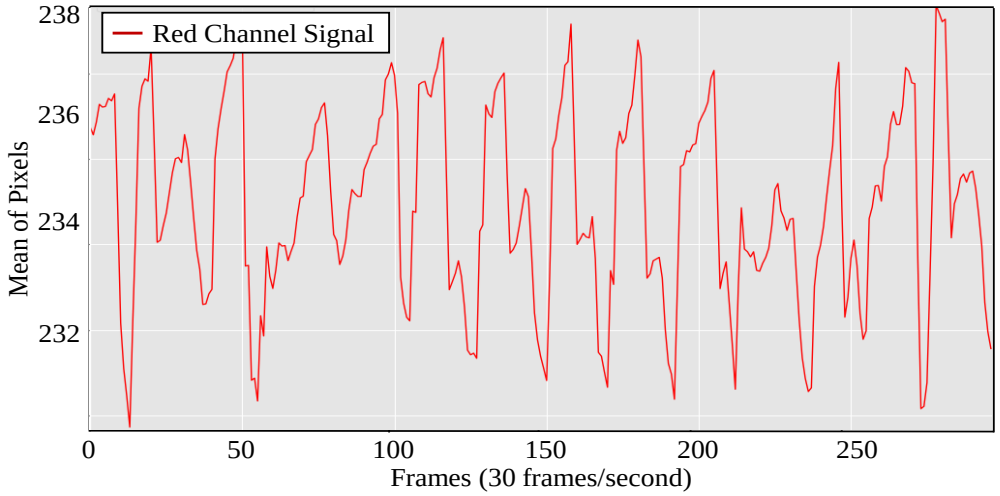

(a)

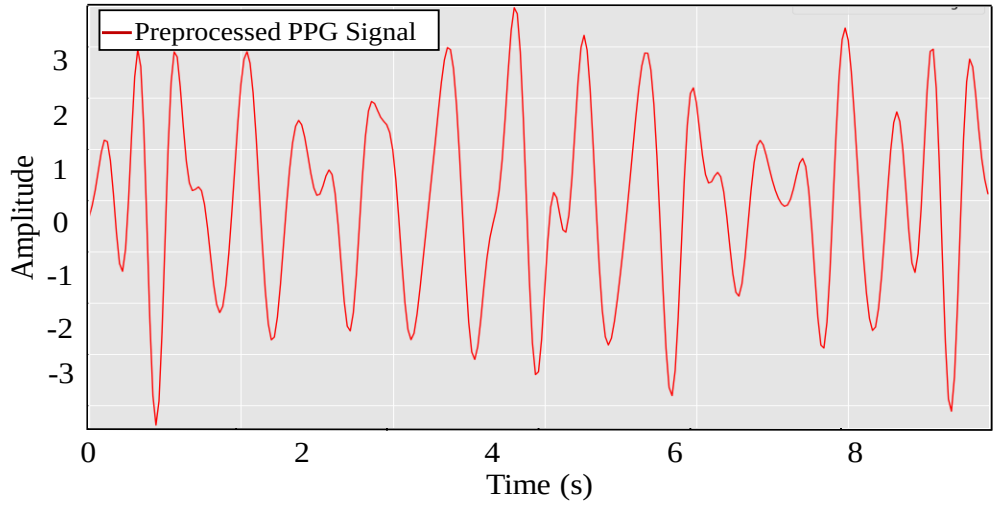

(b)

Figure 4.6: Generation of PPG signal from fingertip video using the mean of pixels of each frame above threshold: (a) raw PPG signal from fingertip video, (b) filtered PPG signal.

the PPG value of the i^{th} frame is measured by (4.3) as the mean of the pixels with intensity above the specific threshold. The PPG signal is acquired by plotting the computed mean of pixels from each frame, as shown in Figure 4.6.

$$threshold_i = \frac{1}{2}(intensity^i_{max} + intensity^i_{min}) \tag{4.2}$$

$$PPG[i] = \frac{1}{total\_pixels} \sum_{i=1}^{total\_pixels} intensity_i > threshold_i \tag{4.3}$$

Before feature extraction, the raw PPG signal was preprocessed to minimize noise and motion artifacts. Then, the Butterworth bandpass filter [74] was applied to the generated PPG

Algorithm 1: Generation of PPG signal from fingertip videos using the mean of pixels of each frame above threshold

Input: N-number of videos
Output: *PPGSig*-generated PPG Signal
/* For NIR-0850 lighting condition, capture 15sec(30fps) videos with Nexus-6p smartphone */
for $i \leftarrow 1$ **to** N **do**
  /* First 60 frames (2s) and last 90 frames (3s) are discarded */
  Extract only 300 frames for each video;
  /* Initialization list: *ListH* */
  List of select highest intensity channel *ListH*;
  for $j \leftarrow 1$ **to** 300 **do**
    /* Calculate the threshold value for each $Frame_j$ */
    $threshold_j = 0.5 * (intensity^j_{max} + intensity^j_{min})$;
    /* Calculate *MeanR*, *MeanG*, *MeanB* */
    Average value of red channel *MeanR*;
    Average value of green channel *MeanG*;
    Average value of blue channel *MeanB*;
    for $k \leftarrow 1$ **to** 3 **do**
      if $channel_k$ *is red* ***AND*** $channel_k \geq threshold_k$ **then**
        MeanR $\leftarrow$ average intensity for red channel from $Frame_j$;
      else if $channel_k$ *is green* ***AND*** $channel_k \geq threshold_k$ **then**
        MeanG $\leftarrow$ average intensity for green channel from $Frame_j$;
      else
        MeanB $\leftarrow$ average intensity for blue channel from $Frame_j$;
    /* Calculate maximum value of channels */
    $MaxvalC \leftarrow \max(MeanR, MeanG, MeanB)$;
    /* Append maximum value from three channels to list: *ListH* */
    $ListH_j \leftarrow MaxvalC$;
  /* Generate PPG signals: $PPGSig_i$ */
  $PPGSig_i \leftarrow butterworthFilter(ListH)$;
return *PPGSig*

signal with frequency per second (fps) = 30, minimum blood pulse per minute (BPM_L)= 40, maximum blood pulse per minute (BPM_H) = 220, and order = [2, 3, 4, 6]. Nyquist frequency is as half of the frame per second (fps/2), which is equivalent to 30/2=15. Therefore, Lower-frequency (lowcut) = $(BPM\_L/60) \times (2/fps)$ and Higher-frequency (highcut) = $(BPM\_H/60) \times (2/fps)$. The order is selected empirically. The preprocessed PPG signals using Butterworth bandpass filter with various order are shown in Figure 4.7. From Figure 4.7 ((a) and (b)), it is shown that the dicrotic notch and diastolic peak are not properly found when using orders 2 and 3 respectively. On the other hand, the dicrotic notch and diastolic

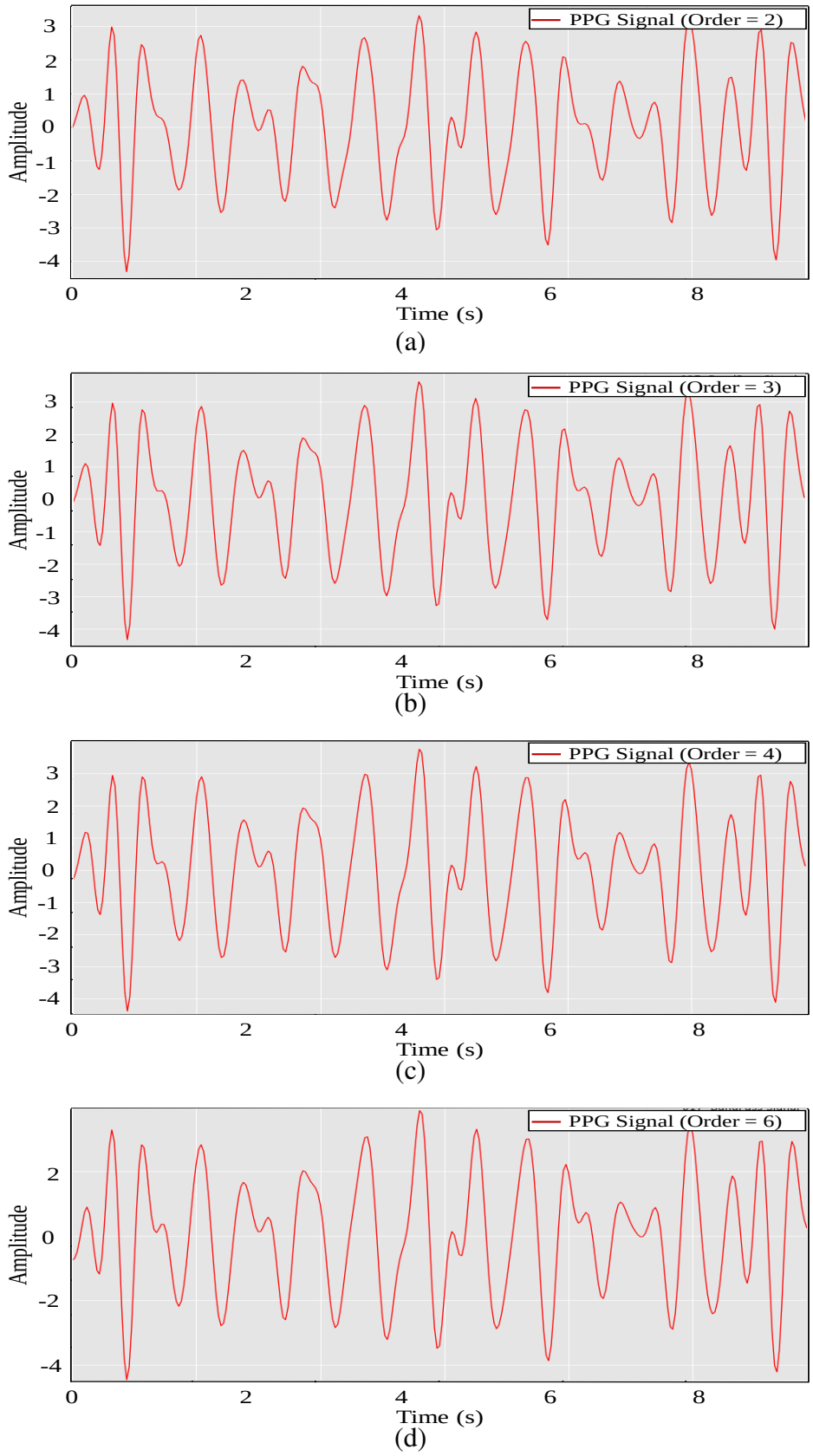

Figure 4.7: Preprocessed PPG signal using Butterworth bandpass filter with different order.

peak are found properly when using orders = 6 but it decreases the amplitude of the PPG signal (Figure 4.7(d)). In this work, the Butterworth bandpass filter performs better with order = 4, and the preprocessed PPG signal looks close to the ideal PPG signal as shown in Figure 4.7(c). The pipeline of the PPG signal generation from video data is described algorithmically in Algorithm 1.

4.5 PPG Cycle Selection and Feature Extraction

In this study, one single PPG cycle is needed to extract the features. PPG signals are continuous and repetitive waveforms that usually contain the same information. A peak detection algorithm was applied to detect each systolic peak. Therefore, PPG signals were segmented into single cycle period from 10s *time_frame* PPG signal, representing a single heartbeat. Each single-period PPG signal might look relatively different for each person, but

Algorithm 2: PPG cycle detection and selection algorithm

Input: Series of continuous PPG signal S_{PPG}
Output: Best single PPG cycle B_{PPG}

$List_C \leftarrow \phi$;
/* $List_C \leftarrow$ list of valid cycle */
/* **Cycle Detection** */
while *time_frame* ≥ 10 **do**
    /* Duration of each PPG signal is 10s */
    Detect each cycle C_{PPG} **in** S_{PPG} **as follows:** ;
    Consider starting point (S_p), dicrotic notch (z), and ending point (E_p) are consecutive minima (M_a);
    Consider systolic peak (x), and diastolic peak (y) are consecutive maxima (M_x);
    Use *find_peak* from the NumPy module of python to detect the peaks of PPG signal and reduce the search time;
    /* Valid PPG cycle check */
    if C_{PPG} *contains* (M_a, M_x) **then**
        /* PPG cycle must has typical critical features like systolic peak, dicrotic notch or diastolic peak. */
        if *x is greater than y and z is greater than* (S_p, E_p) **then**
            $List_C \leftarrow List_C \cup C_{PPG}$;
        else
            Discard C_{PPG};
    else
        Discard C_{PPG};
/* **Cycle Section** */
$B_{PPG} \leftarrow max_x(List_C)$;
/* PPG cycle $List_C$ with the maximum systolic amplitude x */
return B_{PPG};

they all have the same characteristics. Normally, 10*s time_frame* PPG signals contain two or more cycles, and the best one PPG cycle (B_{PPG}) was detected automatically by using the peak detection algorithm in Algorithm 2. In a PPG cycle, starting point, dicrotic notch, and ending point are consecutive minima and systolic peak, and diastolic peak are consecutive maxima points. If a PPG cycle contains consecutive maxima and minima, it is a valid PPG cycle. All the valid PPG cycle C_{PPG} are stored in a list. Therefore, C_{PPG} with the highest positive systolic peak is extracted from the S_{PPG} because of its highest intensity changes. The selected PPG cycle B_{PPG} in a S_{PPG} is depicted in Figure 4.8. This single PPG cycle B_{PPG} was analyzed to extract characteristic features.

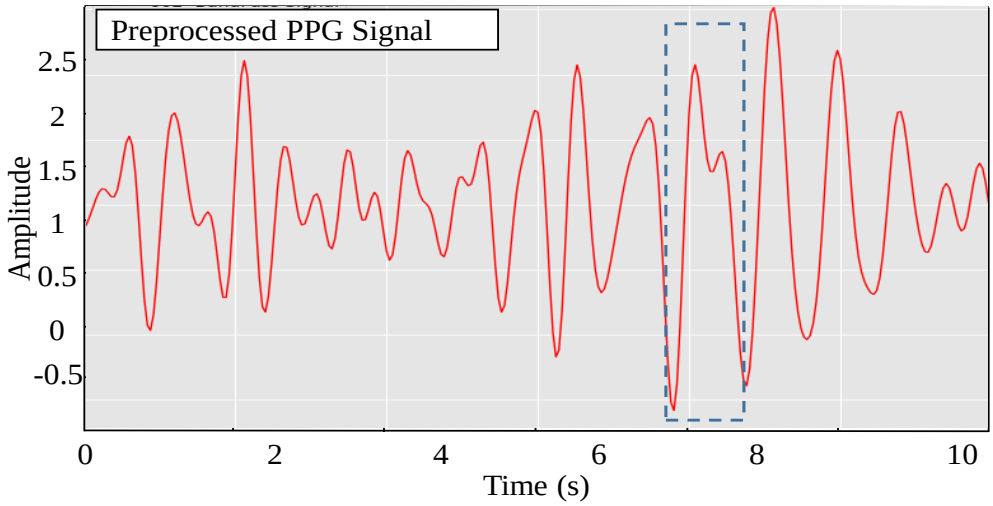

(a) Detection of PPG cycle

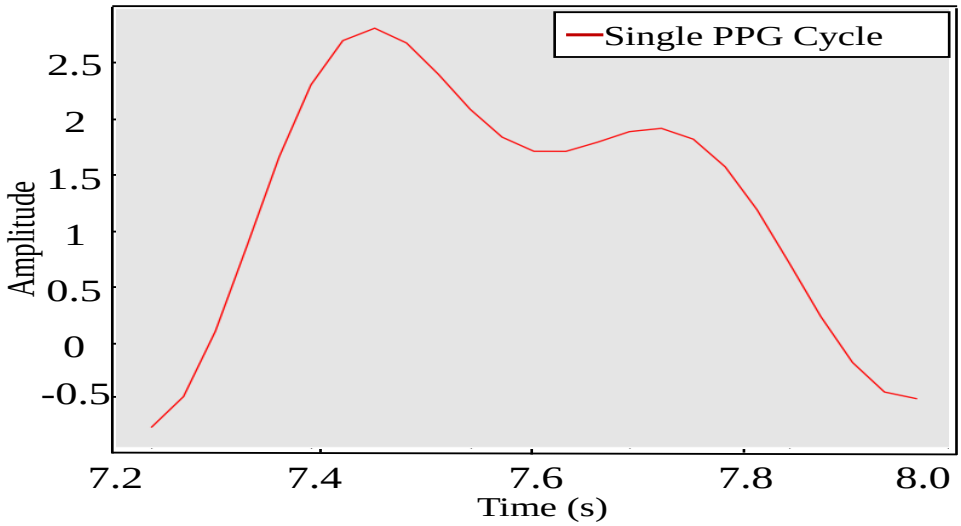

(b) Selection of single PPG cycle

Figure 4.8: Detection and selection of one single PPG cycle from continuous waveform of PPG signal.

After selecting the best PPG cycle, 34 features were extracted from B_{PPG}, its first derivatives (velocity-PPG′ or VPPP), and its first derivatives (acceleration-PPG″ or APPG), as well

as Fourier transformation [75, 76]. The extracted features are divided into four categories: amplitude related features (f_1 to f_5, f_{15} to f_{18}, and f_{23} to f_{25}), time domain features (f_6 to f_{12}, f_{19} to f_{22}, and f_{26} to f_{28}), frequency domain features (f_{29} to f_{34}) and other features (f_{12} to f_{14}). Additionally, Age (f_{35}) and Gender (f_{36}) are added to the feature set. Block diagram of the feature extraction process is depicted in Figure 4.9. Extracted features are described below:

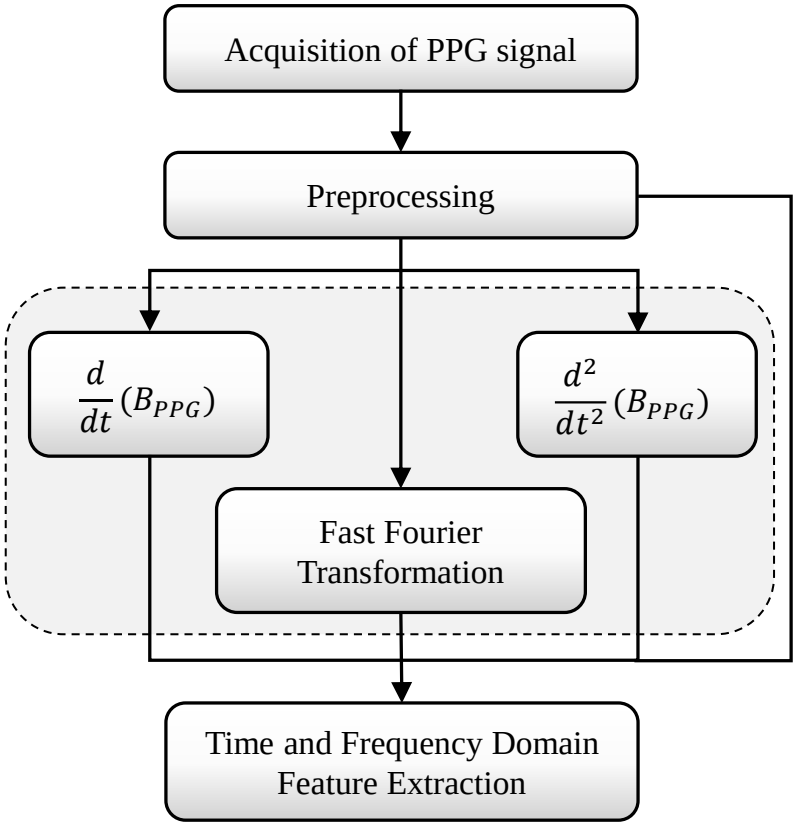

Figure 4.9: Block diagram of feature extraction.

The features extracted from the B_{PPG} signal are graphically illustrated in Figure 4.10 and described below:

- **($\mathbf{f}_1$) Maximum slope:** Amplitude at maximum slop on the up-rise of the PPG signal. c denotes the maximum slope in Figure 4.10.
- **($\mathbf{f}_2$) Magnitude of systolic peak:** Systolic peak is the maxima of a PPG wave [77]. x denotes the magnitude of systolic peak in Figure 4.10.
- **($\mathbf{f}_3$) Magnitude of diastolic peak:** The diastolic peak is the continually first maxima after systolic peak [77]. y denotes the magnitude of diastolic peak in Figure 4.10.
- **($\mathbf{f}_4$) Magnitude of dicrotic notch:** Inside the PPG wave, there is a time-split diverse between systolic and diastolic cardiac levels to create a dicrotic notch. z denotes the magnitude of dicrotic notch in Figure 4.10.
- **($\mathbf{f}_5$) Magnitude of inflection point:** Point of the inflection in the PPG pulse is determined by the local maximum in the first derivative wave after the first peak. d denotes the

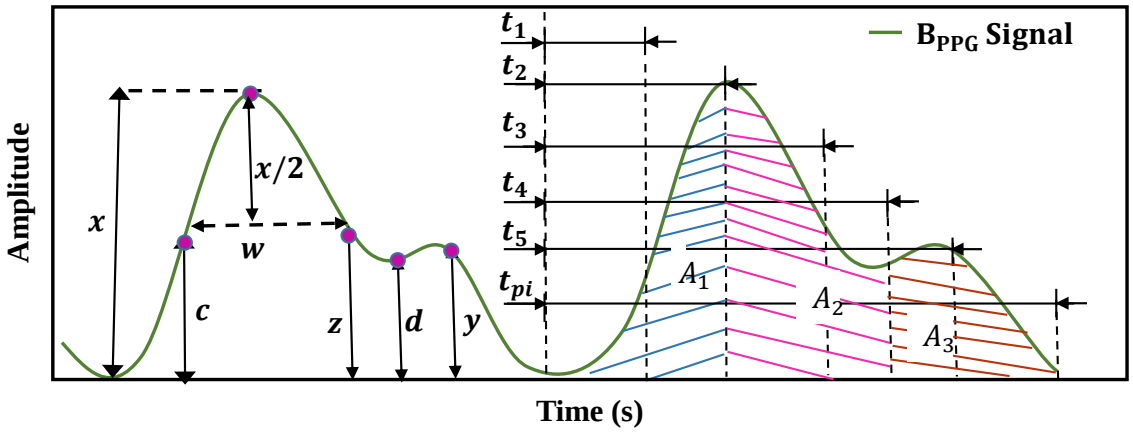

Figure 4.10: The characteristic features acquired from the B_{PPG} signal.

magnitude of dicrotic notch in Figure 4.10.

(f_6) Max. slope time: In the horizontal axis, time to maximum slop on the up-rise of the B_{PPG} signal. It is denoted as t_1 in Figure 4.10.

(f_7) Systolic peak time: In the horizontal axis, from the start of wave to systolic peak is known as systolic peak time. It is denoted as t_2 in Figure 4.10.

(f_8) Dicrotic notch time: In the horizontal axis, from the start of a wave to dicrotic notch is known as dicrotic notch time. It is denoted as t_3 in Figure 4.10.

(f_9) Inflection point time: In the horizontal axis, from the start of a wave to inflection point is known as inflection point time. It is denoted as t_4 in Figure 4.10.

(f_{10}) Diastolic peak time: In the horizontal axis, from the start of a wave to diastolic peak is known as diastolic peak time. It is denoted as t_5 in Figure 4.10.

(f_{11}) Pulse Interval: The length involving start and end of PPG wave. pulse interval is denoted by t_{pi} in Figure 4.10.

(f_{12}) Pulse width at half amplitude: It is denoted by w is shown in Figure 4.10. Awad et al. [78] used the pulse width as the pulse width at the half height of the systolic peak. They have suggested that the pulse width correlates with the systemic vascular resistance better than the systolic amplitude.

(f_{13}) Inflection Point Area ratio (IPA): The pulse region within the PPG wave is considered as the entire area. Pulse area has been split into two areas at inflection point, area A_1+A_2 and area A_3 (Figure 4.10) [79]. The ratio of the two areas can be utilized as an indicator of the entire peripheral resistance [80]. This IPA can be defined as follows:

$$IPA = A_3/(A_1+A_2)$$

(f_{14}) Stress-induced vascular response index (sVRI): The sVRI used as a cognitive load and stress indicator is described as the proportion of two areas at the systolic peak that divided the pulse area (Figure 4.10) [55]. sVRI is calculated from the PPG signal and

can be defined as follows:

$$sVRI = (A_2 + A_3)/A_1$$

The first derivative is hardly used in literature. The first derivative PPG is also known as velocity plethysmogram (VPPG or PPG′). The features extracted from the fist derivative of the B_{PPG} signal are graphically illustrated in Figure 4.11 and described below:

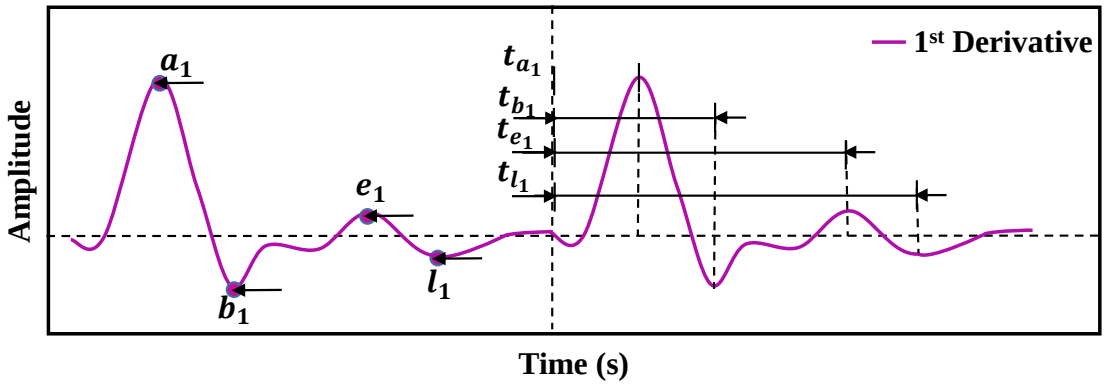

Figure 4.11: The characteristic features acquired from the first derivative of B_{PPG} signal.

($\mathbf{f}_{15}$) a_1**:** First peak of the volume change velocity. a_1 denotes the first peak intensity of VPPG in Figure 4.11.

($\mathbf{f}_{16}$) b_1**:** First valley of the volume change velocity. b_1 denotes the first valley intensity of VPPG in Figure 4.11.

($\mathbf{f}_{17}$) e_1**:** Second peak of the volume change velocity. e_1 denotes the second peak intensity of VPPG in Figure 4.11.

($\mathbf{f}_{18}$) l_1**:** Second valley of the volume change velocity. l_1 denotes the second valley intensity of VPPG in Figure 4.11.

($\mathbf{f}_{19}$) t_{a_1}**:** Interval time from begining to point a_1 for first derivative of B_{PPG}.

($\mathbf{f}_{20}$) t_{b_1}**:** Interval time from begining to point b_1 for first derivative of B_{PPG}.

($\mathbf{f}_{21}$) t_{e_1}**:** Interval time from begining to point e_1 for first derivative of B_{PPG}.

($\mathbf{f}_{22}$) t_{l_1}**:** Interval time from begining to next point l_1 for first derivative of B_{PPG}.

The second derivative is more commonly used than the first derivative. The second derivative of PPG is also referred to as the acceleration plethysmogram (APPG or PPG″) since it is an indicator associated with the acceleration of the bloodstream in the finger [81]. The features extracted from the second derivative of the B_{PPG} signal are graphically illustrated in Figure 4.12 and described below:

($\mathbf{f}_{23}$) a_2**:** First peak of the volume change acceleration. a_2 denotes the first peak intensity of APPG in Figure 4.12.

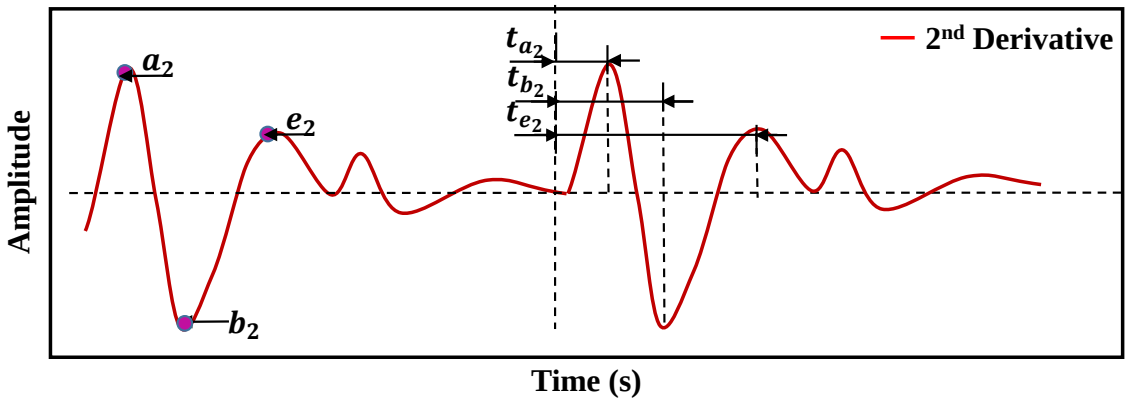

Figure 4.12: The characteristic features acquired from the second derivative of B_{PPG} signal.

(**f**$_{24}$) b_2**:** First valley of the volume change acceleration. b_2 denotes the first valley intensity of APPG in Figure 4.12.

(**f**$_{25}$) e_2**:** Second peak of the volume change acceleration. e_2 denotes the second peak intensity of APPG in Figure 4.12.

(**f**$_{26}$) t_{a_2}**:** Interval time from begining to point a_2 for APPG.

(**f**$_{27}$) t_{b_2}**:** Interval time from begining to point b_2 for APPG.

(**f**$_{28}$) t_{e_2}**:** Interval time from begining to point e_2 for APPG.

The Fast Fourier Transformation (FFT) is used to extract amplitude and frequency domain features from the B_{PPG} wave. Only first three component from the FFT were considered. These tell us the dominant frequencies in the cycle. The features extracted from the FFT of the B_{PPG} signal are graphically illustrated in Figure 4.13 and described below:

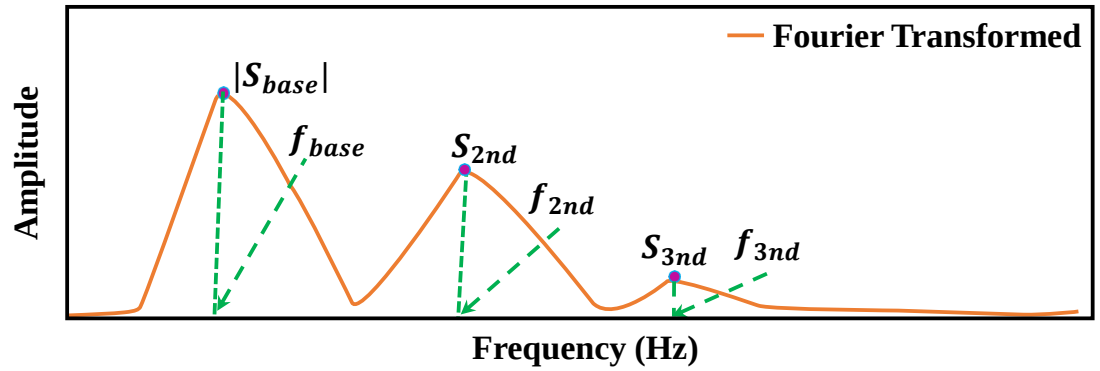

Figure 4.13: Illustration of frequency-domain features from fast fourier transformated B_{PPG} signal.

(**f**$_{29}$) f_{base}**:** Fundamental component frequency acquired from FFT of the B_{PPG} signal.

($\mathbf{f}_{30}$) $|s_{base}|$**:** Fundamental component magnitude acquired from FFT of the B_{PPG} signal with respect to f_{base}.

($\mathbf{f}_{31}$) f_{2nd}**:** 2^{nd} Harmonic frequency acquired from FFT of the B_{PPG} signal. Such that, $f_{base} < f_{2nd}$.

($\mathbf{f}_{32}$) $|s_{2nd}|$**:** 2^{nd} Harmonic magnitude acquired from FFT of the B_{PPG} signal with respect f_{2nd}.

($\mathbf{f}_{33}$) f_{3rd}**:** 3^{rd} Harmonic frequency acquired from FFT of the B_{PPG} signal. Such that, $f_{base} < f_{2nd} < f_{3rd}$.

($\mathbf{f}_{34}$) $|s_{3nd}|$**:** 3^{rd} Harmonic magnitude acquired from FFT of the B_{PPG} signal with respect f_{3rd}.

Finally, the demographic features are described as below:

($\mathbf{f}_{35}$) **Age:** Age of the participant (in year). Types and range of glucose level varies with age of the person.

($\mathbf{f}_{36}$) **Gender:** Gender of the participant (1 for male, 0 for female). The normal range for hemoglobin level depend on the age and gender of the person.

4.6 Feature Selection

Feature selection is the most important step before model construction as the prediction power of a model depends on the features. Redundant, irrelevant or partially relevant features can negatively affect model performance. There are several benefits of performing feature selection before developing the model. Firstly, it reduces over-fitting opportunities by discarding redundant features. Secondly, this process discards irrelevant features, which reduces misleading opportunities and improves model accuracy. Lastly, it reduces the number of features, hence reduces the complexity of the algorithm and model train faster. There are a number of feature selection methods for feature selection. In this study, the Maximal Information Coefficient (MIC) technique has been applied to determine the optimal feature set. MIC is a theory-based information measure of reciprocal dependency that may account for various functional and non-functional dependencies between variables [82]. Using this approach, the relationship between the input features and the target variable is established. The highest-scoring attributes are selected as those are most probable to have the most influence on the estimation results. For two discrete vectors, mutual information $MI_D(F,O)$ is defined as:

$$MI_D(F,O) = \sum_{o\in O}\sum_{f\in F} P(f,o)\log\left(\frac{P(f,o)}{P(f)P(o)}\right) \tag{4.4}$$

where, $P(f,o)$ refers to the joint probabilistic mass function of f and o. The marginal mass functions of f and o are $P(f)$ and $P(o)$. For continuous variables, mutual information

$MI_C(F,O)$ is formulated as follows:

$$MI_C(F,O) = \int \int P(f,o) \log(\frac{P(f,o)}{P(f)P(o)}) dfdo \tag{4.5}$$

where, $P(f,o)$ denotes the associated joint probabilistic density and marginal probabilistic density functions are $P(f)$, and $P(o)$, respectively. Directly calculating the probabilistic mass function can be a useful tool for assessing the dependence of two continuous variables; however, it is not always straightforward to do so. So, providing a maximal mutual information searching approach and an optimal data binning method, MIC was created to overcome this problem [83]. Meanwhile, the mutual information can be normalized to a scale from 0 to 1 with the help of MIC, making it easier to evaluate the dependencies and co-relationships between two variables. Consequently, for each pair of colinear features, we eliminated the features with the lower MIC value against hemoglobin and glucose levels, and allowed the other features for further analysis.

The best feature subsets obtained using MIC for blood component levels for various score are tabulated in Tables 4.2, 4.3 and 4.4, respectively. Figure 4.14 demonstrates the score of each features against the output level. To select the optimal feature set, the score value is selected emprically. To select the optimal feature set, the score value is selected empirically. In this study, the score value is set as 0.45, 0.5, and 0.55, respectively. We obtained 28 features for hemoglobin and 29 for glucose, respectively, for score >= 0.45, as shown in Table 4.2. Similarly, for a score >= 0.5, we acquired 22 features for hemoglobin, and 21 for glucose shown in Table 4.3. Finally, for a score >= 0.55, only 8 features were obtained for hemoglobin and 9 features for glucose. When we have chosen features with a score >=0.45 or less, the optimal feature set is close to the original feature set. Hence, it does not influence the results to a large extent. On the other hand, when we have chosen features with a score >=0.55 or more, it discards most of the essential features. Therefore, in this study, the optimal feature sets for hemoglobin and glucose levels are selected using a score >= 0.5.

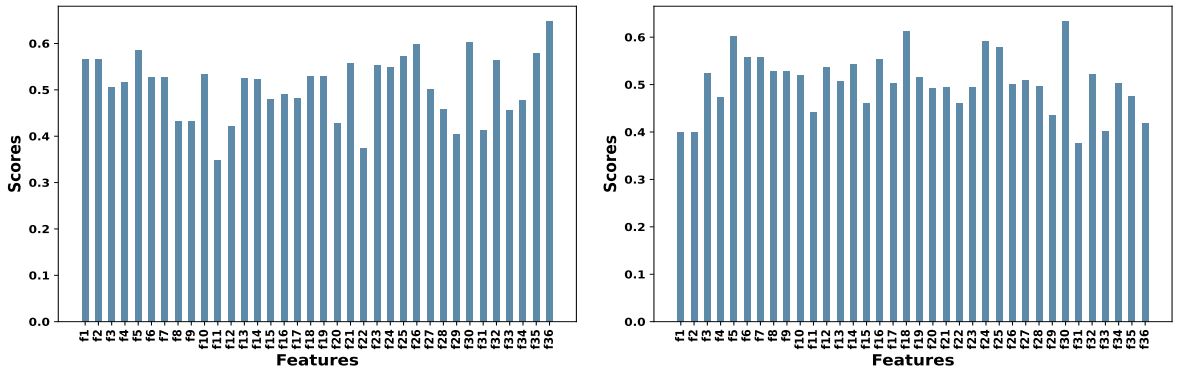

(a) (b)

Figure 4.14: Importance analysis for input features: (a) Hemoglobin, and (b) Glucose

Table 4.2: Selected features using MIC algorithm for hemoglobin and glucose levels when score >= 0.45.

Dataset	Selected Features	Count
Hemoglobin	f_1 f_2 f_3 f_4 f_5 f_6 f_7 f_{10} f_{13} f_{14} f_{15} f_{16} f_{17} f_{18} f_{19} f_{21} f_{23} f_{24} f_{25} f_{26} f_{27} f_{28} f_{30} f_{32} f_{33} f_{34} f_{35} f_{36}	28
Glucose	f_3 f_4 f_5 f_6 f_7 f_8 f_9 f_{10} f_{12} f_{13} f_{14} f_{15} f_{16} f_{17} f_{18} f_{19} f_{20} f_{21} f_{22} f_{23} f_{24} f_{25} f_{26} f_{27} f_{28} f_{30} f_{32} f_{34} f_{35}	29

Table 4.3: Selected features using MIC algorithm for hemoglobin and glucose levels when score >= 0.5.

Dataset	Selected Features	Count
Hemoglobin	f_1 f_2 f_3 f_4 f_5 f_6 f_7 f_{10} f_{13} f_{14} f_{18} f_{19} f_{21} f_{23} f_{24} f_{25} f_{26} f_{27} f_{30} f_{32} f_{35} f_{36}	22
Glucose	f_3 f_5 f_6 f_7 f_8 f_9 f_{10} f_{12} f_{13} f_{14} f_{16} f_{17} f_{18} f_{19} f_{24} f_{25} f_{26} f_{27} f_{30} f_{32} f_{34}	21

Table 4.4: Selected features using MIC algorithm for hemoglobin and glucose levels when score >= 0.55.

Dataset	Selected Features	Count
Hemoglobin	f_1 f_2 f_5 f_{21} f_{23} f_{25} f_{26} f_{30} f_{32} f_{35} f_{36}	11
Glucose	f_5 f_6 f_7 f_{16} f_{18} f_{24} f_{25} f_{30}	8

4.7 Model Construction and Validation

At the first stage, the ANN models were developed to estimate the hemoglobin and glucose levels. The models were trained with 100 epochs, 32 batch size, and a learning rate of 0.01. The hyperparameters used in the proposed ANN models are shown in Table 4.5.

Furthermore, two independent models using deep neural network were constructed for more accurate estimation of hemoglobin and glucose levels. The DNN models were trained with 100 epochs, 32 batch size, and a learning rate of 0.01. To facilitate the training processing and update the parameter of parameters of DNN, Adam was used as optimizer function. The hyperparameters used in the proposed DNN based models are shown in Table 4.6. The DNN models were trained and tested with both all features and MIC-based selected features for each blood component level.

The $K-$fold cross-validation (KCV) is one of the most popular methods that can be used for selection and evaluation of the performance of machine learning techniques with less

Table 4.5: Hyperparameters and their values used in ANN models.

Parameters	**Status**
Batch size	32
Learning rate α	0.01
The number of hidden layers	1
The number of nodes at hidden layer	73
The number of nodes at input layer	36 or optimal feature set
The number of node at output layer	2
Activation function	ReLU, Linear

Table 4.6: Hyperparameters and their values used in DNN models.

Parameters	**Status**
Batch size	32
Learning rate α	0.01
The number of hidden layers	4
The number of nodes at 4 hidden layers	(150, 200, 250, 300)
Dropout at 2nd and 4th hidden layers	(0.25, 0.5)
The number of nodes at input layer	36 or optimal feature set
The number of node at output layer	2
Activation function	ReLU, Linear
Optimizer	Adam

variance than a single split train test set [84, 85]. It is operated by dividing the data samples into K-parts (e.g., $K = 5$ or $K = 10$) [86]. In this study, the 10-fold cross-validation method is used to construct and evaluate the performances of DNN models. At first, reference Hb values and PPG characteristics features (age and gender were also included as features) of 93 subjects are divided into 10 almost equal subgroups or folds to train and test the model. In each iteration, 9 subgroups are used for training the model, and the rest one is used for testing the model. This process went on until 10 iterations are completed. After 10 times of training and testing, the reliable Hb estimation model was established. The same procedure was followed for the remaining DNN models to estimate Gl level. The final performance metric is determined as in (4.6).

$$E_M = \frac{1}{K} \times \sum_{n=1}^{K} E_n \tag{4.6}$$

where, E_M is the final evaluation metric for each model and $E_n \in \mathbb{R}$, $n = 1, 2, \ldots, K$ is the evaluation metric for each fold. To investigate the competency of the new developed model, the dataset are also trained with classical regression methods such as linear regression (LR), and support vector regression (SVR) using the same input conditions as ANN and DNN

models.

4.8 Conclusion

In this chapter, we have presented a non-invasive hemoglobin and glucose levels assessment process using the PPG signal generated from a fingertip video, which was captured using a smartphone under near-infrared LED light. Analyzing the PPG signals, we have extracted characteristic features from PPG signals and its derivatives as well as Fourier Transformed signals. Finally, we have applied features selection algorithms to select optimal feature set and fed to developed models for estimation. In the next chapter, we will present the experimental analysis of our proposed method.

CHAPTER V

Experimental Results and Discussions

5.1 Introduction

In this chapter experimental analysis, performance and effectiveness of the proposed method will be explained briefly. Finally, the estimation accuracy of the proposed system is compared with other prominent works to validate the performance of our proposed system.

5.2 Experimental Setup

The results presented in this work are generated using a single computer (Asus $X556U$, $Intel® \ \ Core(TM) \ \ i5-72000U$, central processing unit with $2.50GHz$, 8.0 GB Random Access Memory, and Nvidia GeForce $940MX$) with $Windows-10$ operating system. The machine learning and deep neural network models are implemented in Python 3.6 with a computing environment named Spyder, available in Anaconda.

5.3 Performance Measurement Metrics

The performance of our proposed method is evaluated using four indices such as coefficient of determination (R^2), mean absolute error (MAE), mean squared error (MSE), and root mean square error (RMSE). If $o_1, o_2, \cdots, o_n$ are n reference values and $\hat{o}_1, \hat{o}_2, \cdots, \hat{o}_n$ are the corresponding estimated values, then the mathematics formulas are as follows:

- $\boldsymbol{R^2}$: A statistical measure of how close the data are to the fitted regression line. The coefficient of determination is a measure that evaluates the ability of prediction of a model.

$$R^2 = 1 - \frac{\sum_{i=1}^{n}(o_i - \hat{o}_i)^2}{\sum_{i=1}^{n}(o_i - \bar{o})^2} \tag{5.1}$$

  where, $\bar{o} = \frac{1}{n}\sum_{0}^{n-1} o_i$

- **MAE**: A error metric corresponding to the expected value of the absolute error or loss. It is the quantity that helps to determine how close predictions are to the final results.

$$MAE = \frac{1}{n}\sum_{i=1}^{n}|o_i - \hat{o}_i| \tag{5.2}$$

- **MSE**: A error metric corresponding to the expected value of the squared (quadratic) error or loss.

$$MSE = \frac{1}{n}\sum_{i=1}^{n}(o_i - \hat{o}_i)^2 \tag{5.3}$$

- **RMSE**: It is a frequently used measure of the differences between values predicted by a model or an estimator and the true values. In other words, it tells you how concentrated the data is around the line of best fit.

$$RMSE = \sqrt{\frac{1}{n}\sum_{i=1}^{n}(o_i - \hat{o}_i)^2} \tag{5.4}$$

5.4 Robustness Performance of Models

The performance of the proposed method has been evaluated with four performance measurement indices: R^2, MAE, MSE, and RMSE It is noteworthy that the proximity of R^2 to 1 indicates the strength of the relationship between model outputs and reference values. The RMSE and MSE show relative errors, and the MAE represents the absolute error. R^2 shows a correlation of blood component (Hb and Gl) levels with input features. The higher values of R^2 indicate that the model performed well with the input datasets.

In this study, a total of 93 subjects (59 male (63.5%) and 34 female (36.5%)) were studied ranging in age from 0 to 69 years. The range of reference blood hemoglobin values for this study from 7.9 g/dL to 21.49 g/dL, with μ = 12.933 g/dL and σ = 2.137 g/dL. Similarly, for the clinically measured individual sample, the range of reference blood glucose values for this study from 3.33 mmol/L to 21.11 mmol/L, with μ = 6.64 mmol/L and σ = 2.97 mmol/L.

In this study, the models were trained and validated using the two datasets. The first dataset consisted of extracted PPG signal's features (PPG-34), whereas the PPG signal was generated using the mean of pixels of each frame. Second dataset consisted of features extracted from PPG (PPG-34), whereas the PPG signal was generated using the mean of pixels of each frame above the threshold. Age and Gender were also added as features. The datasets were PPG-$HbGl_1$ and PPG-$HbGl_2$, respectively.

5.4.1 PPG-$HbGl_1$ Dataset

In the beginning stage, the models were trained and tested using PPG-$HbGl_1$ dataset with all the features for each blood component level (Hb and Gl). A 10-fold cross-validation technique was used to verify the models, where each fold contains the reference Hb and measurement Hb levels. Therefore, the mean performance of the models were determined following that. The same procedure was followed for the blood Gl level. Initially, the ANN models were applied to estimate the blood Hb and Gl levels. Later, the DNN models were developed to improve the estimated accuracy. The PPG-$HbGl_1$ dataset were also trained using classical

regression models such as linear regression (LR) and support vector regression (SVR). Table 5.1 illustrates that our proposed DNN models perform better compared to other models with all features. The estimated accuracies of proposed DNN models using all features are R^2 = 0.874 and MAE = 0.414 for Hb level as wll as 0.850 and 0.566 for Gl level, respectively. Table 5.2 shows the reference blood component levels (Hb and Gl) and their respective estimated values with DNN models with all features. Here, we present the first ten subjects' data.

Furthermore, the MIC feature selection algorithm was applied to determine the optimal feature set. It is essential to reduce the likelihood of models being overfitted. After using

Table 5.1: Performance measurement of blood component levels using various models with all features (PPG-HbGl$_1$ dataset).

Model	With all features							
	Hb				Gl			
	R^2	MAE	MSE	RMSE	R^2	MAE	MSE	RMSE
LR	0.188	0.727	0.878	0.937	0.201	0.843	2.696	1.642
SVR	0.247	0.695	0.815	0.902	0.320	0.954	2.136	1.461
ANN	0.842	0.284	0.726	0.852	0.817	0.439	1.610	1.269
Proposed(DNN)	**0.874**	**0.414**	**0.581**	**0.762**	**0.850**	**0.566**	**1.319**	**1.148**

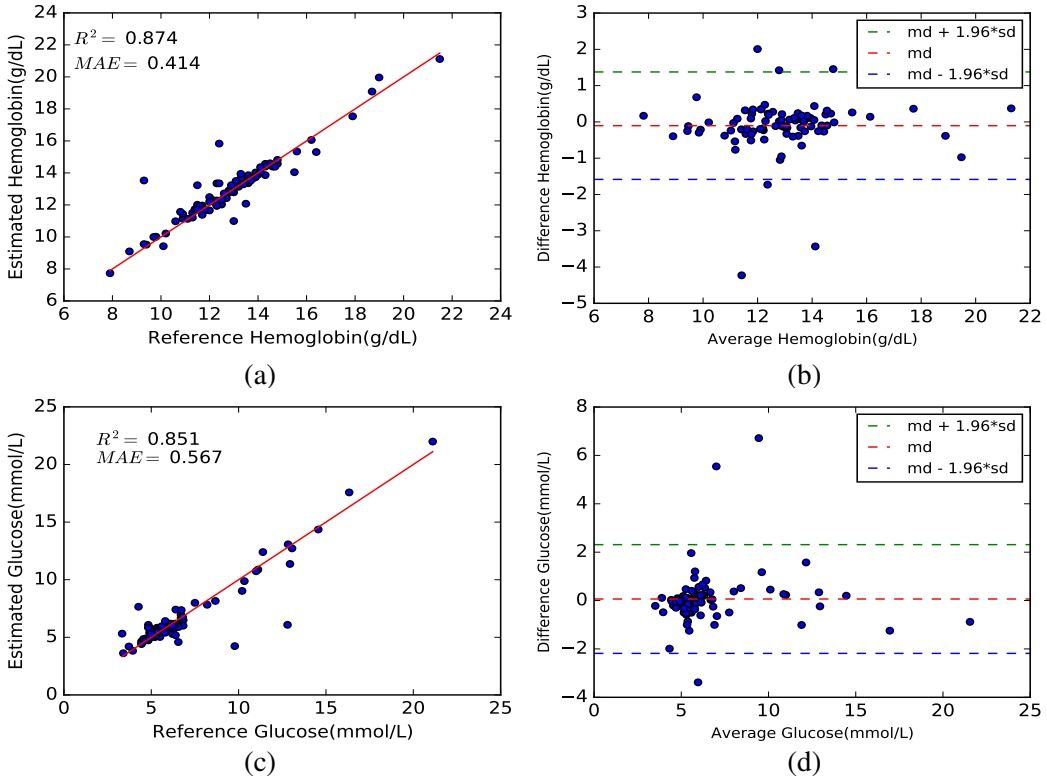

Figure 5.1: Relationship and agreement (Bland-Altman) plots between estimated values and reference values of Hb and Gl levels at testing stage for DNN models with all features using PPG-HbGl$_1$ dataset: (a) relationship (Hb), (b) agreement (Hb), (c) relationship (Gl), and (d) agreement (Gl).

Table 5.2: Estimated Blood component levels (Hb and Gl) from the DNN models with their corresponding reference values and their difference using PPG-HbGl$_1$ dataset with all features.

Patient ID	Hemoglobin			Glucose		
	Reference Hb	Estimated Hb	Difference	Reference Gl	Estimated Gl	Difference
01	11.9	11.68	0.22	4.44	4.64	-0.2
02	12.1	12.33	-0.23	6.61	6.08	0.53
03	14.3	14.57	-0.27	6.55	4.59	1.96
04	13.6	13.36	0.24	4.66	4.9	-0.24
05	12.3	13.35	-1.05	6.28	5.72	0.56
06	11.3	11.51	-0.21	5.28	5.32	-0.04
07	13.7	13.69	0.01	4.94	5.8	-0.86
08	14.5	14.6	-0.1	8.67	8.16	0.51
09	14.6	14.4	0.2	4.83	6.08	-1.25
10	12.8	12.78	0.02	11.39	12.4	-1.01

the MIC algorithm on the PPG-HbGl$_1$ dataset, the number of features was reduced from 36 to 22 for Hb and 21 for Gl, respectively. From Table 4.3, it is shown that the optimal features are varied with regard to measurement level. It is occurred due to different features are correlated to different blood component levels. Therefore, the optimal features were fed to the ANN and DNN models to estimate the blood component levels. Models were validated using 10-fold cross-validation for each reference blood component level. According to the obtained results in Table 5.3, the estimated accuracies of proposed DNN models with MIC algorithm are R^2 = 0.963, and MAE = 0.243 for Hb level as wll as 0.964 and 0.303 for Gl level, respectively. Overall, it is clear that the proposed method (DNN+MIC) provides the best-estimated accuracy compared to classical algorithms and ANN models, as well as DNN models with all features. Table 5.4 shows the reference blood component levels (Hb and Gl) and their respective estimated values with DNN models with all features.

Table 5.3: Performance measurement of blood component levels using various models with optimal feature set via MIC feature selection algorithm (PPG-HbGl$_1$ dataset).

Model	With selected features via MIC (22 features for Hb and 21 features for Gl)							
	Hb				Gl			
	R^2	MAE	MSE	RMSE	R^2	MAE	MSE	RMSE
LR	0.281	0.675	0.815	0.924	0.352	0.924	2.201	1.365
SVR	0.421	0.517	0.684	0.769	0.592	0.674	1.799	1.024
ANN	0.901	0.278	0.467	0.683	0.898	0.507	1.031	0.988
Proposed(DNN+MIC)	**0.963**	**0.243**	**0.164**	**0.405**	**0.964**	**0.303**	**0.320**	**0.566**

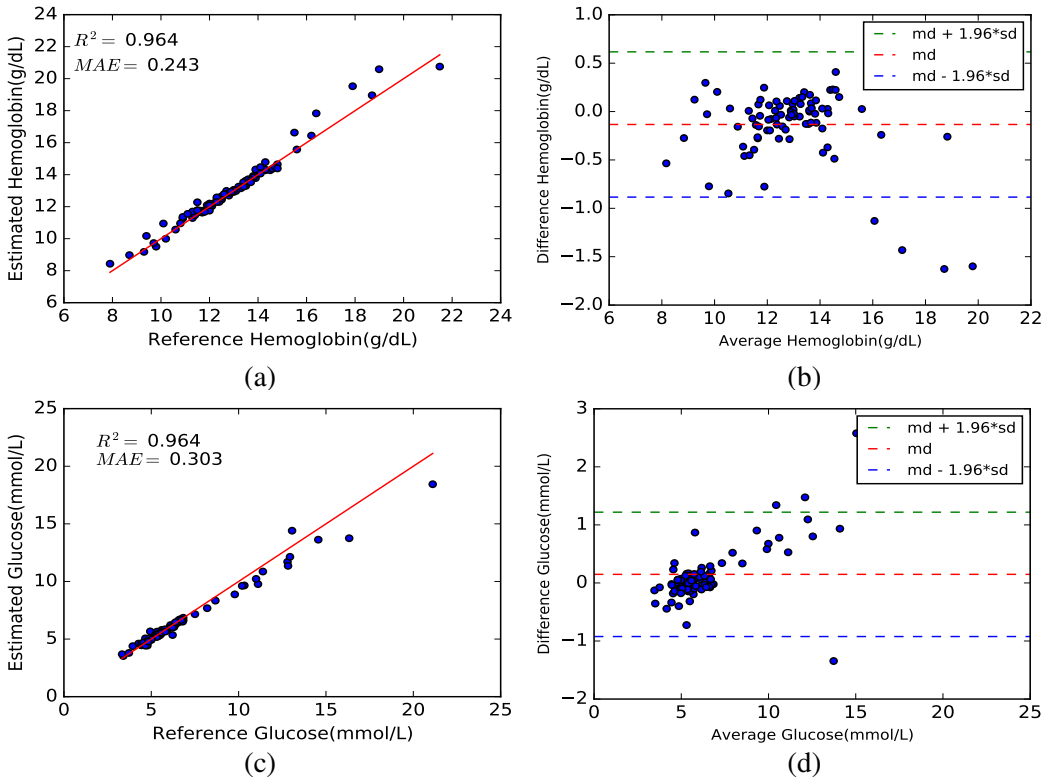

Figure 5.2: Relationship and agreement (Bland-Altman) plots between estimated values and reference values of Hb and Gl levels at testing stage for DNN models with MIC selected features using PPG-HbGl$_1$ dataset: (a) relationship (Hb), (b) agreement (Hb), (c) relationship (Gl), and (d) agreement (Gl).

A relationship between the reference values and estimated values for blood component

Table 5.4: Estimated Blood component levels (Hb and Gl) from the DNN models with their corresponding reference values and their difference using PPG-HbGl$_1$ dataset with MIC selected features.

Patient ID	Hemoglobin			Glucose		
	Reference Hb	Estimated Hb	Difference	Reference Gl	Estimated Gl	Difference
01	11.9	12.14	-0.24	4.44	4.45	-0.01
02	12.1	12.55	-0.45	6.61	6.71	-0.1
03	14.3	14.51	-0.21	6.55	5.55	1.0
04	13.6	13.51	0.09	4.66	5.21	-0.55
05	12.3	13.26	-0.96	6.28	5.7	0.58
06	11.3	10.81	0.49	5.28	5.28	-0.0
07	13.7	13.45	0.25	4.94	5.82	-0.88
08	14.5	14.5	-0.0	8.67	8.91	-0.24
09	14.6	14.02	0.58	4.83	5.9	-1.07
10	12.8	13.09	-0.29	11.39	11.6	-0.21

levels has been established to understate the above results better. Figure 5.1 ((a), and (c)) and Figure 5.2 ((a), and (c)) show the correlation-based comparison between estimated values and reference values for Hb and Gl levels for DNN models, respectively. Furthermore, Figure 5.3 ((b), and (d)) and Figure 5.4 ((b), and (d)) depict the Bland-Altman plot for determining the distance between the measurement value and the reference value. Bland-Altman plot [87] establishes limits of agreement to specify the relationship between these values. The plots show that a higher percentage of measurement values are within the limits of agreement ($md \pm 1.96 * sd$). At 95%, confidence interval, the limits of agreement for Hb with all features were [-1.584, 1.376], and [-0.884, 0.617] for MIC selected features. Similarly, the limits of agreement for Gl with all features were [-2.184, 2.311], and [-0.923, 1.218] for MIC selected features.

5.4.2 PPG-HbGl$_2$ Dataset

In the second stage, the models were trained and tested using PPG-HbGl$_1$ dataset with all the features for each blood component level. We have applied the same procedure in this stage, like for PPG-HbGl$_1$ dataset. Initially, the ANN models were developed to estimate the Hb and Gl level, respectively. Further, two independent DNN models were developed to improve the estimation performance. The proposed DNN based models were trained and tested with all the features for each blood component level. The PPG-HbGl$_2$ dataset was also trained using classical regression models such as LR and SVR, respectively. Table 5.5 illustrates the comparison of estimation results for our proposed DNN models with other modes for all features. The estimated accuracies of proposed DNN models using all features are $R^2 = 0.897$ and MAE = 0.357 for Hb level as wll as 0.874 and 0.545 for Gl level, respectively. Table 5.6 illustrate the reference blood component levels (Hb and Gl) and their respective estimated values with DNN models with all features.

Table 5.5: Performance measurement of blood component levels using various models with all features (PPG-HbGl$_2$ dataset).

Model	With all features							
	Hb				Gl			
	R^2	MAE	MSE	RMSE	R^2	MAE	MSE	RMSE
LR	0.188	0.727	0.878	0.937	0.201	0.843	2.696	1.642
SVR	0.247	0.695	0.815	0.902	0.320	0.954	2.136	1.461
ANN	0.853	0.386	0.678	0.823	0.848	0.490	1.294	1.137
Proposed(DNN)	**0.897**	**0.357**	**0.470**	**0.686**	**0.874**	**0.545**	**1.102**	**1.049**

Besides, the MIC feature selection algorithm was applied to PPG-HbGl$_2$ dataset to determine the optimal feature set. After using the MIC algorithm on the PPG-HbGl$_2$ dataset, the number of features was reduced from 36 to 22 for Hb and 21 for Gl, respectively.

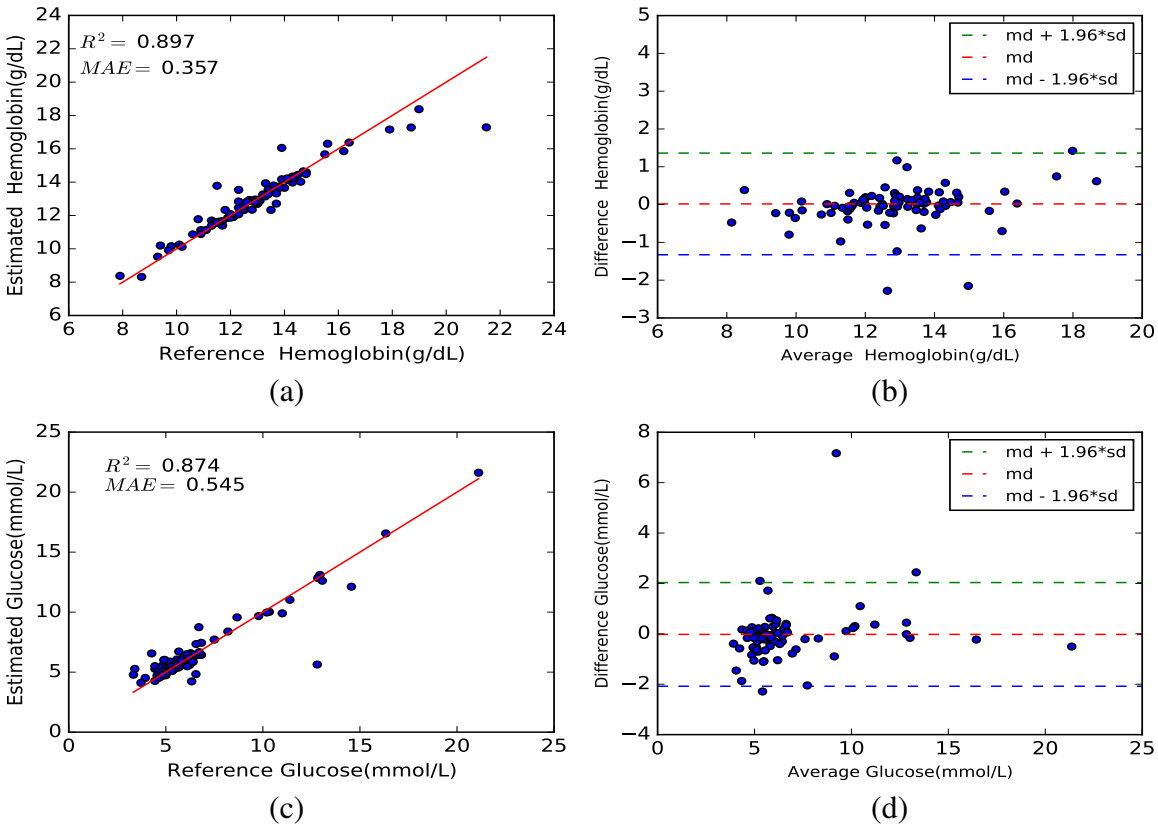

Figure 5.3: Relationship and agreement (Bland-Altman) plots between estimated values and reference values of Hb and Gl levels at testing stage for DNN models with all features using PPG-HbGl$_2$ dataset: (a) relationship (Hb), (b) agreement (Hb), (c) relationship (Gl), and (d) agreement (Gl).

Table 5.6: Estimated Blood component levels (Hb and Gl) from the DNN models with their corresponding reference values and their difference using PPG-HbGl$_2$ dataset with all features (more details in Appendix Table A.2).

Patient ID	Hemoglobin			Glucose		
	Reference Hb	Estimated Hb	Difference	Reference Gl	Estimated Gl	Difference
01	11.9	12.2	-0.3	4.44	4.15	0.29
02	12.1	11.87	0.23	6.61	6.25	0.36
03	14.3	14.1	0.2	6.55	4.9	1.65
04	13.6	13.47	0.13	4.66	4.82	-0.16
05	12.3	13.64	-1.34	6.28	6.14	0.14
06	11.3	12.01	-0.71	5.28	5.1	0.18
07	13.7	13.75	-0.05	4.94	5.77	-0.83
08	14.5	14.43	0.07	8.67	8.98	-0.31
09	14.6	14.67	-0.07	4.83	5.14	-0.31
10	12.8	12.57	0.23	11.39	11.39	-0.0

Table 5.7: Performance measurement of blood component levels using various models with optimal feature set via MIC feature selection algorithm (PPG-HbGl$_2$ dataset).

Model	With selected features via MIC (22 features for Hb and 21 features for Gl)							
	Hb				Gl			
	R^2	MAE	MSE	RMSE	R^2	MAE	MSE	RMSE
LR	0.281	0.675	0.815	0.924	0.352	0.924	2.201	1.365
SVR	0.421	0.517	0.684	0.769	0.592	0.674	1.799	1.024
ANN	0.922	0.195	0.359	0.599	0.901	0.407	0.824	0.768
Proposed(DNN+MIC)	**0.969**	**0.235**	**0.139**	**0.373**	**0.968**	**0.263**	**0.280**	**0.529**

Therefore, the optimal features were fed to the ANN and DNN models to estimate the blood component levels. According to the obtained results in Table 5.7, the estimated accuracies of proposed DNN models with MIC algorithm are R^2 = 0.969, and MAE = 0.235 for Hb level as wll as 0.968 and 0.263 for Gl level, respectively. Overall, it is clear that the proposed method (DNN+MIC) provides the best-estimated accuracy compared to classical algorithms and DNN models with all features. Table 5.8 demonstrate the reference blood component levels (Hb and Gl) and their respective estimated values with DNN models with all features.

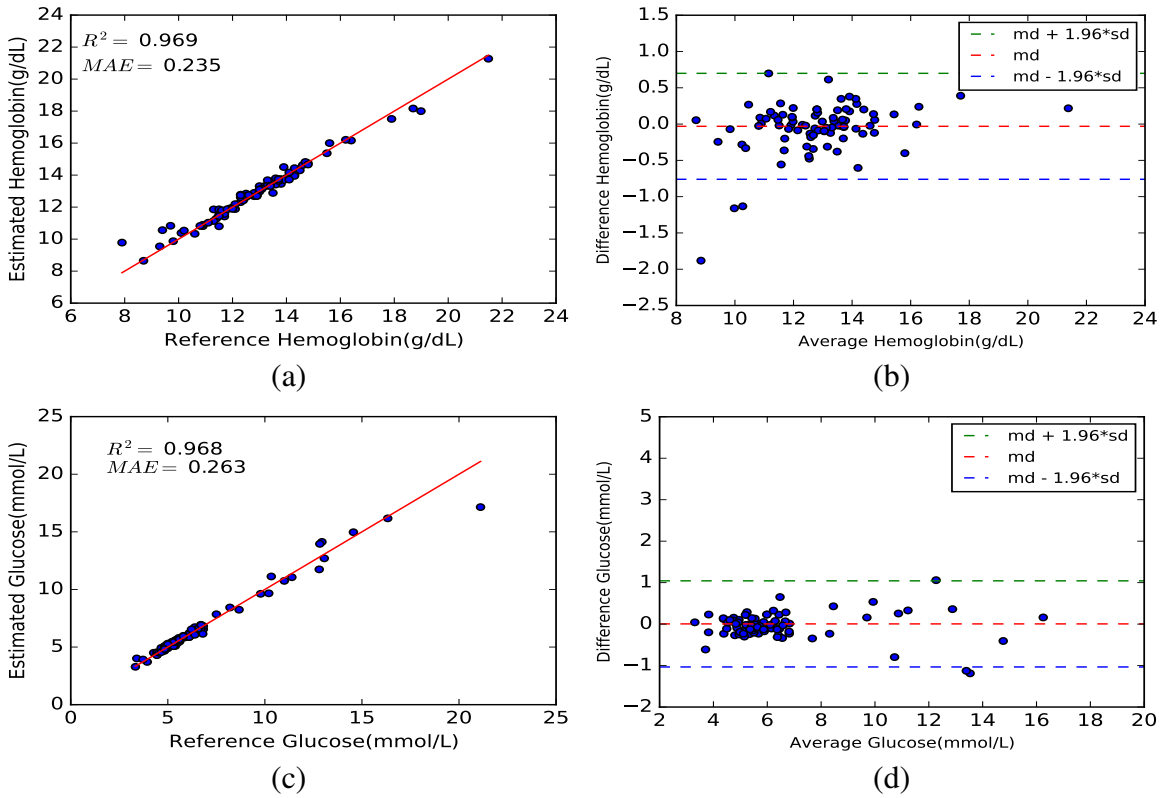

Figure 5.4: Relationship and agreement (Bland-Altman) plots between estimated values and reference values of Hb and Gl levels at testing stage for DNN models with MIC selected features using PPG-HbGl$_2$ datase: (a) relationship (Hb), (b) agreement (Hb), (c) relationship (Gl), and (d) agreement (Gl).

Moreover, it can be noted that our proposed method perform betther for PPG-HbGl$_2$ dataset compared to PPG-HbGl$_1$ dataset. From Table 5.3, it is shown that the estimated accuracies of proposed method (DNN+MIC) are R^2 = 0.963, and MAE = 0.243 for Hb level as wll as 0.964 and 0.303 for Gl level, respectively, for PPG-HbGl$_1$ dataset. On the other hand, Table 5.3, it is illustrated that the estimated accuracies of proposed method (DNN+MIC) are R^2 = 0.969, and MAE = 0.235 for Hb level as wll as 0.968 and 0.263 for Gl level, respectively, for PPG-HbGl$_2$ dataset. In the PPG-HbGl$_2$ dataset, PPG signals were generated from only valid frames. Erroneous frames (frames that are too dark due to incorrect placement of the finger on the camera and NID-LED) were rejected using the threshold value. Therefore, characteristic features were extracted from the more accurate PPG signals. Hence, PPG-HbGl$_2$ dataset provides better results than PPG-HbGl$_2$ dataset.

Table 5.8: Estimated Blood component levels (Hb and Gl) from the DNN models with their corresponding reference values and their difference using PPG-HbGl$_2$ dataset with MIC selected features (more details in Appendix Table A.2).

Patient ID	Hemoglobin			Glucose		
	Reference Hb	Estimated Hb	Difference	Reference Gl	Estimated Gl	Difference
01	11.9	11.92	-0.02	4.44	4.37	0.07
02	12.1	11.79	0.31	6.61	7.12	-0.51
03	14.3	14.47	-0.17	6.55	5.71	0.84
04	13.6	13.63	-0.03	4.66	4.79	-0.13
05	12.3	12.45	-0.15	6.28	5.65	0.63
06	11.3	11.43	-0.13	5.28	5.56	-0.28
07	13.7	13.65	0.05	4.94	5.09	-0.15
08	14.5	14.53	-0.03	8.67	8.65	0.02
09	14.6	14.94	-0.34	4.83	5.19	-0.36
10	12.8	12.77	0.03	11.39	10.84	0.55

Figure 5.3 ((a), and (c)) and Figure 5.4 ((a), and (c)) show the correlation-based comparison between estimated values and reference values for Hb and Gl levels, respectively, for PPG-HbGl$_2$ dataset. Furthermore, Figure 5.3 ((b), and (d)) and Figure 5.4 ((b), and (d)) depict the Bland-Altman plot for determining the distance between the measurement value and the reference value. At 95%, confidence interval, the limits of agreement for Hb with all features were [-1.327, 1.361], and [-0.761, 0.699] for MIC selected features. Similarly, the limits of agreement for Gl with all features were [-2.080, 2.035], and [-1.033, 1.0434] for MIC selected features using PPG-HbGl$_2$ dataset.

5.5 Unsuccessful Case Example

From Table 5.8, it is shown that the difference between estimated and reference Gl values for fingertip video (ID 3) is higher compared to other samples. The generation of good PPG signals from fingertip video and feature extraction influences the accuracy of estimation models. The PPG signal can be corrupted due to the movement of the fingertip during the fingertip video collection. Figure 5.5 shows the generated PPG signal from the fingertip video of Patient ID 3. The PPG signal is slightly affected by noise and motion artefacts, which influences further analysis. Hence, it increases the estimated error. However, the error between estimated and reference Gl values is 0.84, it seems it is not too high and the proposed system can be applied in clinical trials. More deatails about PPG signal and its extracted features is presented in Appendix Table A.2.

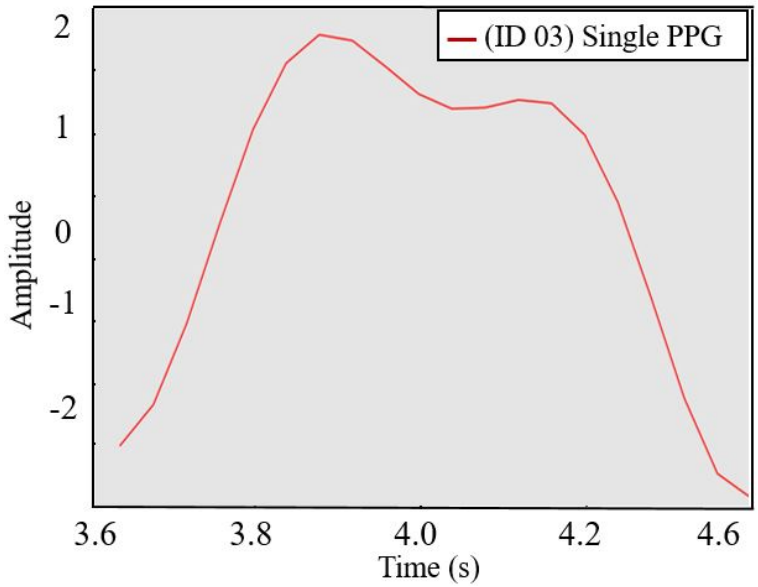

Figure 5.5: Selected PPG signal generated from fingertip video.

5.6 Comparison with Other Works

A comparison study is drawn in Table 5.9 for estimating hemoglobin and glucose levels to validate our contributions with respect to existing works that used the smartphone camera for data collection.

Looking at individual related works in Table 5.9, Wang et al. [35] developed a smartphone-based application named as HemaApp (FDA-approved device) to measure Hb level non-invasively. The authors captured fingertip video data from 31 subjects using Nexus-5p, used the SVR model, and achieved highest relationship with correlation coefficient (R) of 0.82. In [24], the same authors improved the configuration of hardware and used the LR model,

Table 5.9: Comparison of our proposed DNN based models with several exiting smartphone-based non-invasive methods.

Authors	Purpose	#Sub	Smartphone	Captured	Algorithm(s)	Performance
Wang et al. [35]		31	Nexus-5p		SVR	$R = 0.82$
Edward et al. [24]		32	Nexus-6p		LR	$R = 0.62$
Anggraeni and Fatoni [36]		20	Asus Zen-Fone 2 Laser		LR	$R^2 = 0.81$
Hasan et al. [37]		75	Nexus-4p		ANN	$R^2 = 0.93$
Zhang et al. [39]		14	iPhone 6s Plus		DT, BT and KNN	$Acc =$ 86.2%
Chowdhury et al. [38]		18	iPhone 7 Plus		PCR	$SEP =$ $18.31 mg/dL$
Glovanni et al. [51]		113	iPhone 4s, Huawei p7		KNN	$R = 0.65$
Proposed Method		93	Nexus-6p		DNN	**$R^2 = 0.969$** **$R^2 = 0.968$**

* = Hemoglobin, = Glucose, = Video, = Image, SVR = Support Vector Regression, LR = Linear Regression, ANN = Artificial Neural Network, DT = Decision Tree, BT = Bagged Trees, KNN = K-nearest neighbor, PCR = Principal Component Regression, SEP = Standard Error of Prediction, DNN = Deep Neural Network.

and achieved a Pearson correlation of 0.62. Anggraeni and Fatoni [36] developed LR model using conjunctiva image of 20 participants captured by Asus ZenFone 2 and estimated the Hb level that highly correlated with clinical Hb value and gained a relationship with R^2 of 0.81. In [37], the authors developed a smartphone-based application named as SmartHeLP to measure the Hb concentration in blood. In this case, they collected 75 fingertip video data via Nexus-4p smartphone and applied in the ANN model, and achieved relationship with R^2 of 0.93. Zhang et al. [39] developed a system for the estimation of blood Gl level based on smartphone fingertip video. The authors acquired the PPG signal from video, used subspace KNN classifier and obtained the accuracy $Acc = 86.2\%$. Chowdhury et al. [38] proposed a smartphone-based approach to estimate the blood Gl level in a non-invasive. The authors recorded the fingertip video, converted the frames into PPG signal, applied PCR algorithm on the extracted features, and achieved a SEP as low as 18.31 mg/dL. Glovanni et al. [51] designed a non-invasive system to screen the anemia using conjunctiva image. The authors used two smartphones, iPhone 4s and Huawei p7 to collect the conjunctiva images from 113 subjects, applied KNN model on the extracted features and achieved the R values as 0.65. However, it is difficult to compare existing works related to this filed due to different datasets, hardware configuration, and smartphone to collect the data from various parts of the subject's

body and different evaluation criteria.

In our proposed method, we have used a smartphone device (Nexus-6p) to capture the fingertip video data, generated PPG signal from fingertip videos, applied various preprocessing techniques to minimize the noise, extracted 34 features from PPG signal, applied MIC feature selection algorithm to select optimal feature set and developed DNN based models to estimate the hemoglobin, and glucose levels more accurately. It is almost clear from these results that our proposed methodology can be used in real-time healthcare applications.

5.7 Conclusion

In this study, we have trained and validated our proposed method using two datasets. Our proposed DNN model, along with MIC-based selected features, performed better than the model with all features using the PPG-HbGl$_2$ dataset for estimating haemoglobin and glucose levels. We have also compared our proposed method with existing methods that used smartphones to acquire data.

CHAPTER VI

Conclusion and Recommendation

6.1 Conclusions

Regular hemoglobin and glucose level monitoring prevents long-term and short-term consequences for anemic and diabetic patients, respectively. This paper has proposed a novel non-invasive method to estimate blood Hb and Gl levels with smartphone PPG signals extracted from fingertip videos and deep neural network model. It provides an excellent basis for observing real-time blood haemoglobin and glucose levels at home. For this purpose, fingertip video is first captured using a smartphone camera while the fingertip is illuminated using the NIR-LED kit. As the smartphone's camera and flashlight are not designed for this purpose, several difficulties have been faced in capturing noise-free data. We have also discussed the challenges faced in the data collection stage and outlined some recommendations for noise-free data collection. Secondly, the frames are converted into PPG signals and then 34 features extracted from the PPG signal, its derivatives, and Fourier form. Age and gender of each subject are also added as features. Thirdly, appropriate features are selected using the MIC feature selection technique. Finally, two independent DNN models are developed to estimate hemoglobin and glucose using these features and validated with 10-fold cross-validation. In this work, we wanted to compare classical regression models with DNN models for medical data. The results are compared with classical regression models to evaluate the performance of the DNN-based model. The DNN model and the MIC feature selection method provided the highest estimated accuracy in measuring the Hb and Gl levels. The results indicate that our proposed technique can be used in clinical practice.

6.2 Recommendation for Future Work

Non-invasive techniques are an attractive research field. We believe that a clinically accurate and acceptable model can be developed based on the work reported here if we can create acceptable signal-to-noise ratios and rigorous signal processing techniques and analyze larger data sets from patients with the full range of hemoglobin and glucose levels seen in clinical practice. We suggest that pursuing the following strategies will likely lead to the definition of a more accurate and acceptable clinical estimation model.

- Minimizing signal-to-noise ratios (SNR) in PPG signals generation and feature extraction to improve the accuracy of estimation models [88].

- Developing the PPG generation algorithm using the ratio of superimposition averaging template and pulse wave [89], optimized differential extraction method [90], and dynamic spectrum method [91].
- Constructing a well-designed hardware system, to reduce the pressure of the fingertip-pad on the smartphone camera and finger movement that can alter the waveform of the PPG signal [92].
- Providing a smartphone application to measure hemoglobin and glucose and transferring high computational processes from smartphones to the cloud [93].

REFERENCES

1. Ashish Kumar, Rama Komaragiri, Manjeet Kumar, et al. A review on computation methods used in photoplethysmography signal analysis for heart rate estimation. *Archives of Computational Methods in Engineering*, 29(2):921–940, 2022.

2. Hemoglobin ranges: Normal, symptoms of high and low levels. `https://www.medicinenet.com/hemoglobin/article.htm`, 2019. Accessed: 2019-02-03.

3. Bruno De Benoist, Mary Cogswell, Ines Egli, and Erin McLean. Worldwide prevalence of anaemia 1993-2005; who global database of anaemia. 2008.

4. Who | database on anemia. `https://www.who.int/vmnis/database/anaemia/en/`, 2019. Accessed: 2019-02-03.

5. Saul S Morris, Marie T Ruel, Roberta J Cohen, Kathryn G Dewey, Bénédicte de la Brière, and Mohammed N Hassan. Precision, accuracy, and reliability of hemoglobin assessment with use of capillary blood. *The American journal of clinical nutrition*, 69(6):1243–1248, 1999.

6. Md Kamrul Hasan, Nazmus Sakib, Richard R Love, and Sheikh I Ahamed. Analyzing the existing noninvasive hemoglobin measurement techniques. In *2017 IEEE 8th Annual Ubiquitous Computing, Electronics and Mobile Communication Conference (UEMCON)*, pages 442–448. IEEE, 2017.

7. J Lourdes Albina Nirupa and V Jagadeesh Kumar. Non-invasive measurement of hemoglobin content in blood. In *2014 IEEE International Symposium on Medical Measurements and Applications (MeMeA)*, pages 1–5. IEEE, 2014.

8. Juan Li and Chandima Fernando. Smartphone-based personalized blood glucose prediction. *ICT Express*, 2(4):150–154, 2016.

9. Konstantinos Papatheodorou, Maciej Banach, Eleni Bekiari, Manfredi Rizzo, and Michael Edmonds. Complications of diabetes 2017. *Journal of diabetes research*, 2018, 2018.

10. Anjali D Deshpande, Marcie Harris-Hayes, and Mario Schootman. Epidemiology of diabetes and diabetes-related complications. *Physical therapy*, 88(11):1254–1264, 2008.

11. World Health Organization et al. Classification of diabetes mellitus. Technical report, World Health Organization, 2019.

12. Joseph Largay. Case study: new-onset diabetes: how to tell the difference between type 1 and type 2 diabetes. *Clinical Diabetes*, 30(1):25–26, 2012.

13. I Osiecka and T Pałko. Overview of some non-invasive spectroscopic methods of glucose level monitoring. *Acta Bio-Optica et Informatica Medica. Inżynieria Biomedyczna*, 22(1):1–8, 2016.

14. Healthy blood glucose levels: Targets, extremes, and lifestyle tips. `https://www.medicalnewstoday.com/articles/249413.php`. Accessed: 2019-02-03.

15. D Naumann and R Meyers. Encyclopedia of analytical chemistry. *John Wiley & Sons, Chichester, UK*, pages 102–131, 2000.

16. Praful P Pai, Pradyut K Sanki, Sudeep K Sahoo, Arijit De, Sourangshu Bhattacharya, and Swapna Banerjee. Cloud computing-based non-invasive glucose monitoring for diabetic care. *IEEE Transactions on Circuits and Systems I: Regular Papers*, 65(2):663–676, 2017.

17. Srinivasan Lekha and M Suchetha. Real-time non-invasive detection and classification of diabetes using modified convolution neural network. *IEEE journal of biomedical and health informatics*, 22(5):1630–1636, 2017.

18. James G Hamilton. Needle phobia: a neglected diagnosis. *Journal of Family Practice*, 41(2):169–182, 1995.

19. Megan Parker, Zhen Han, Elizabeth Abu-Haydar, Eric Matsiko, Damien Iyakaremye, Lisine Tuyisenge, Amalia Magaret, and Alexandre Lyambabaje. An evaluation of hemoglobin measurement tools and their accuracy and reliability when screening for child anemia in rwanda: A randomized study. *PloS one*, 13(1):e0187663, 2018.

20. Anke Sieg, Richard H Guy, and M Begoña Delgado-Charro. Noninvasive and minimally invasive methods for transdermal glucose monitoring. *Diabetes technology & therapeutics*, 7(1):174–197, 2005.

21. Jorge Blasco, Thomas M Chen, Juan Tapiador, and Pedro Peris-Lopez. A survey of wearable biometric recognition systems. *ACM Computing Surveys (CSUR)*, 49(3):43, 2016.

22. Francesco Rundo, Sabrina Conoci, Alessandro Ortis, and Sebastiano Battiato. An advanced bio-inspired photoplethysmography (ppg) and ecg pattern recognition system for medical assessment. *Sensors*, 18(2):405, 2018.

23. Jyoti Yadav, Asha Rani, Vijander Singh, and Bhaskar Mohan Murari. Prospects and limitations of non-invasive blood glucose monitoring using near-infrared spectroscopy. *Biomedical signal processing and control*, 18:214–227, 2015.

24. Edward J Wang, William Li, Junyi Zhu, Rajneil Rana, and Shwetak N Patel. Noninvasive hemoglobin measurement using unmodified smartphone camera and white flash. In *2017 39th Annual International Conference of the IEEE Engineering in Medicine and Biology Society (EMBC)*, pages 2333–2336. IEEE, 2017.

25. Sungjun Kwon, Hyunseok Kim, and Kwang Suk Park. Validation of heart rate extraction using video imaging on a built-in camera system of a smartphone. In *2012 Annual International Conference of the IEEE Engineering in Medicine and Biology Society*, pages 2174–2177. IEEE, 2012.

26. Rajalakshmi Nandakumar, Shyamnath Gollakota, and Nathaniel Watson. Contactless sleep apnea detection on smartphones. In *Proceedings of the 13th annual international conference on mobile systems, applications, and services*, pages 45–57. ACM, 2015.

27. Fen Miao, Nan Fu, Yuan-Ting Zhang, Xiao-Rong Ding, Xi Hong, Qingyun He, and Ye Li. A novel continuous blood pressure estimation approach based on data mining techniques. *IEEE journal of biomedical and health informatics*, 21(6):1730–1740, 2017.

28. Md Asaf-uddowla Golap, S. M. Taslim Uddin Raju, Md Rezwanul Haque, and M. M. A Hashem. Hemoglobin and glucose level estimation from ppg characteristics features of fingertip video using mggp-based model. *Biomedical Signal Processing and Control*, 67:102478, 2021.

29. John Allen. Photoplethysmography and its application in clinical physiological measurement. *Physiological measurement*, 28(3):R1, 2007.

30. Jermana Moraes, Matheus Rocha, Glauber Vasconcelos, José Vasconcelos Filho, Victor de Albuquerque, and Auzuir Alexandria. Advances in photopletysmography signal analysis for biomedical applications. *Sensors*, 18(6):1894, 2018.

31. Neelamshobha Nirala, R Periyasamy, Bikesh Kumar Singh, and Awanish Kumar. Detection of type-2 diabetes using characteristics of toe photoplethysmogram by applying support vector machine. *Biocybernetics and Biomedical Engineering*, 39(1):38–51, 2019.

32. Changmok Choi, Byung-Hoon Ko, Jongwook Lee, Seung Keun Yoon, Uikun Kwon, Sang Joon Kim, and Younho Kim. Ppg pulse direction determination algorithm for ppg waveform inversion by wrist rotation. In *2017 39th Annual International Conference of the IEEE Engineering in Medicine and Biology Society (EMBC)*, pages 4090–4093. IEEE, 2017.

33. Jens Kraitl, Ulrich Timm, Hartmut Ewald, and Elfed Lewis. Non-invasive measurement of blood components. In *2011 Fifth International Conference on Sensing Technology*, pages 253–257. IEEE, 2011.

34. Jasmine P Devadhasan, Hyunhee Oh, Cheol Soo Choi, and Sanghyo Kim. Whole blood glucose analysis based on smartphone camera module. *Journal of biomedical optics*, 20(11):117001, 2015.

35. Edward Jay Wang, William Li, Doug Hawkins, Terry Gernsheimer, Colette Norby-Slycord, and Shwetak N Patel. Hemaapp: noninvasive blood screening of hemoglobin using smartphone cameras. In *Proceedings of the 2016 ACM International Joint Conference on Pervasive and Ubiquitous Computing*, pages 593–604. ACM, 2016.

36. MD Anggraeni and A Fatoni. Non-invasive self-care anemia detection during pregnancy using a smartphone camera. In *IOP Conference Series: Materials Science and Engineering*, volume 172, page 012030. IOP Publishing, 2017.

37. Md Kamrul Hasan, Md Munirul Haque, Riddhiman Adib, Jannatul F Tumpa, Azima Begum, Richard R Love, Young L Kim, and I Ahamed Sheikh. Smarthelp: Smartphone-based hemoglobin level prediction using an artificial neural network. In *AMIA Annual Symposium Proceedings*, volume 2018, page 535. American Medical Informatics Association, 2018.

38. Tauseef Tasin Chowdhury, Tahmin Mishma, Saeem Osman, and Tanzilur Rahman. Estimation of blood glucose level of type-2 diabetes patients using smartphone video through pca-da. In *Proceedings of the 6th International Conference on Networking, Systems and Security*, pages 104–108, 2019.

39. Yuwei Zhang, Yuan Zhang, Sarah Ali Siddiqui, and Anton Kos. Non-invasive blood-glucose estimation using smartphone ppg signals and subspace knn classifier. *Elektrotehniski Vestnik*, 86(1/2):68–74, 2019.

40. Nam Bui, Anh Nguyen, Phuc Nguyen, Hoang Truong, Ashwin Ashok, Thang Dinh, Robin Deterding, and Tam Vu. Pho2: Smartphone based blood oxygen level measurement systems using near-ir and red wave-guided light. In *Proceedings of the 15th ACM conference on embedded network sensor systems*, pages 1–14, 2017.

41. Swathi Ramasahayam, K Sri Haindavi, and Shubhajit Roy Chowdhury. Noninvasive estimation of blood glucose concentration using near infrared optodes. In *Sensing Technology: Current Status and Future Trends IV*, pages 67–82. Springer, 2015.

42. A Reşit Kavsaoğlu, Kemal Polat, and M Hariharan. Non-invasive prediction of hemoglobin level using machine learning techniques with the ppg signal's characteristics features. *Applied Soft Computing*, 37:983–991, 2015.

43. Xiaoguong Sun, Jeffrey I Joseph, and Katherine D Crothall. Implantable sensor and system for measurement and control of blood constituent levels, September 19 2000. US Patent 6,122,536.

44. Jonathan S Jahr, Fedor Lurie, Bernd Driessen, Jessica A Davis, Robert Gosselin, and Robert A Gunther. The hemocue®, a point of care b-hemoglobin photometer, measures hemoglobin concentrations accurately when mixedin vitro with canine plasma and three hemoglobin-based oxygen carriers (hboc). *Canadian Journal of Anesthesia*, 49(3):243, 2002.

45. Glucose meter. `https://en.wikipedia.org/wiki/Glucose_meter`, 2019. Accessed: 2019-03-03.

46. Praful P Pai, Pradyut K Sanki, Sudeep K Sahoo, Arijit De, Sourangshu Bhattacharya, and Swapna Banerjee. Cloud computing-based non-invasive glucose monitoring for diabetic care. *IEEE Transactions on Circuits and Systems I: Regular Papers*, 65(2):663–676, 2018.

47. Tanvir Tazul Islam, Md Sajid Ahmed, Md Hassanuzzaman, Syed Athar Bin Amir, and Tanzilur Rahman. Blood glucose level regression for smartphone ppg signals using machine learning. *Applied Sciences*, 11(2):618, 2021.

48. Daniel P Hsu, Alicia J French, Samuel L Madson, John M Palmer, and Vinod Gidvani-Diaz. Evaluation of a noninvasive hemoglobin measurement device to screen for anemia in infancy. *Maternal and child health journal*, 20(4):827–832, 2016.

49. Shyqyri Haxha and Jaspreet Jhoja. Optical based noninvasive glucose monitoring sensor prototype. *IEEE Photonics Journal*, 8(6):1–11, 2016.

50. Raid Saleem Al-Baradie and Anandh Sam Chandra Bose. Portable smart non-invasive hemoglobin measurement system. In *10th International Multi-Conferences on Systems, Signals & Devices 2013 (SSD13)*, pages 1–4. IEEE, 2013.

51. Giovanni Dimauro, Danilo Caivano, and Francesco Girardi. A new method and a non-invasive device to estimate anemia based on digital images of the conjunctiva. *IEEE Access*, 6:46968–46975, 2018.

52. Giovanni Dimauro, Attilio Guarini, Danilo Caivano, Francesco Girardi, Crescenza Pasciolla, and Angela Iacobazzi. Detecting clinical signs of anaemia from digital images of the palpebral conjunctiva. *IEEE Access*, 7:113488–113498, 2019.

53. Daniel Yim, Gladimir VG Baranoski, BW Kimmel, Tenn F Chen, and Erik Miranda. A cell-based light interaction model for human blood. In *Computer Graphics Forum*, volume 31, pages 845–854. Wiley Online Library, 2012.

54. AVJ Challoner. Photoelectric plethysmography for estimating cutaneous blood flow. *Non-invasive physiological measurements*, 1:125–151, 1979.

55. Xiao Zhang, Yongqiang Lyu, Xin Hu, Ziyue Hu, Yuanchun Shi, and Hao Yin. Evaluating photoplethysmogram as a real-time cognitive load assessment during game playing. *International Journal of Human–Computer Interaction*, pages 1–12, 2018.

56. F. Pedregosa, G. Varoquaux, A. Gramfort, V. Michel, B. Thirion, O. Grisel, M. Blondel, P. Prettenhofer, R. Weiss, V. Dubourg, J. Vanderplas, A. Passos, D. Cournapeau, M. Brucher, M. Perrot, and E. Duchesnay. Scikit-learn: Machine learning in Python. *Journal of Machine Learning Research*, 12:2825–2830, 2011.

57. Vladimir N Vapnik. The nature of statistical learning. *Theory*, 1995.

58. Alex J Smola and Bernhard Schölkopf. A tutorial on support vector regression. *Statistics and computing*, 14(3):199–222, 2004.

59. Kristin P Bennett and Olvi L Mangasarian. Robust linear programming discrimination of two linearly inseparable sets. *Optimization methods and software*, 1(1):23–34, 1992.

60. Ye Ren, Ponnuthurai Nagaratnam Suganthan, and Narasimalu Srikanth. A novel empirical mode decomposition with support vector regression for wind speed forecasting. *IEEE transactions on neural networks and learning systems*, 27(8):1793–1798, 2014.

61. Debasish Basak, Srimanta Pal, and Dipak Patranabis. Support vector regression. *Neural Information Processing – Letters and Reviews*, 11, 11 2007.

62. Charu C Aggarwal. Training deep neural networks. In *Neural Networks and Deep Learning*, pages 105–167. Springer, 2018.

63. Ian Goodfellow, Yoshua Bengio, and Aaron Courville. Deep learning. book in preparation for mit press. *URL¡ http://www. deeplearningbook. org*, 1, 2016.

64. Nitish Srivastava, Geoffrey Hinton, Alex Krizhevsky, Ilya Sutskever, and Ruslan Salakhutdinov. Dropout: a simple way to prevent neural networks from overfitting. *The journal of machine learning research*, 15(1):1929–1958, 2014.

65. Bong-Ki Lee and Joon-Hyuk Chang. Packet loss concealment based on deep neural networks for digital speech transmission. *IEEE/ACM Transactions on Audio, Speech, and Language Processing*, 24(2):378–387, 2015.

66. Lisa Carroll and Tatyana R Humphreys. Laser-tissue interactions. *Clinics in dermatology*, 24(1):2–7, 2006.

67. Tsu-Hsun Fu, Shing-Hong Liu, and Kuo-Tai Tang. Heart rate extraction from photoplethysmogram waveform using wavelet multi-resolution analysis. *Journal of medical and biological engineering*, 28(4):229–232, 2008.

68. Liangyou Chen, Andrew T Reisner, and Jaques Reifman. Automated beat onset and peak detection algorithm for field-collected photoplethysmograms. In *2009 Annual International Conference of the IEEE Engineering in Medicine and Biology Society*, pages 5689–5692. IEEE, 2009.

69. Christopher G Scully, Jinseok Lee, Joseph Meyer, Alexander M Gorbach, Domhnull Granquist-Fraser, Yitzhak Mendelson, and Ki H Chon. Physiological parameter monitoring from optical recordings with a mobile phone. *IEEE Transactions on Biomedical Engineering*, 59(2):303–306, 2011.

70. E Jonathan and Martin Leahy. Investigating a smartphone imaging unit for photoplethysmography. *Physiological measurement*, 31(11):N79, 2010.

71. Hongwei Yuan, Sanober Farheen Memon, Thomas Newe, Elfed Lewis, and Gabriel Leen. Motion artefact minimization from photoplethysmography based non-invasive hemoglobin sensor based on an envelope filtering algorithm. *Measurement*, 115:288–298, 2018.

72. Chen Wei, Lei Sheng, Guo Lihua, Chen Yuquan, and Pan Min. Study on conditioning and feature extraction algorithm of photoplethysmography signal for physiological parameters detection. In *2011 4th International Congress on Image and Signal Processing*, volume 4, pages 2194–2197. IEEE, 2011.

73. Lorenz Frey, Carlo Menon, and Mohamed Elgendi. Blood pressure measurement using only a smartphone. *NPJ digital medicine*, 5(1):1–14, 2022.

74. Ayan Chatterjee and Andreas Prinz. Image analysis on fingertip video to obtain ppg. *Biomedical and Pharmacology Journal*, 11(4):1811–1827, 2018.

75. Xiao Zhang, Yongqiang Lyu, Tong Qu, Pengfei Qiu, Xiaomin Luo, Jingyu Zhang, Shunjie Fan, and Yuanchun Shi. Photoplethysmogram-based cognitive load assessment using multi-feature fusion model. *ACM Transactions on Applied Perception (TAP)*, 16(4):19, 2019.

76. Chadi El-Hajj and Panayiotis A Kyriacou. Cuffless blood pressure estimation from ppg signals and its derivatives using deep learning models. *Biomedical Signal Processing and Control*, 70:102984, 2021.

77. Daniel McDuff, Sarah Gontarek, and Rosalind W Picard. Remote detection of photoplethysmographic systolic and diastolic peaks using a digital camera. *IEEE Transactions on Biomedical Engineering*, 61(12):2948–2954, 2014.

78. Aymen A Awad, Ala S Haddadin, Hossam Tantawy, Tarek M Badr, Robert G Stout, David G Silverman, and Kirk H Shelley. The relationship between the photoplethysmographic waveform and systemic vascular resistance. *Journal of clinical monitoring and computing*, 21(6):365–372, 2007.

79. ERJ Seitsonen, IKJ Korhonen, MJ Van Gils, M Huiku, JMP Lötjönen, KT Korttila, and AM Yli-Hankala. Eeg spectral entropy, heart rate, photoplethysmography and motor responses to skin incision during sevoflurane anaesthesia. *Acta Anaesthesiologica Scandinavica*, 49(3):284–292, 2005.

80. L Wang, Emma Pickwell-MacPherson, YP Liang, and YT Zhang. Noninvasive cardiac output estimation using a novel photoplethysmogram index. In *2009 Annual International Conference of the IEEE Engineering in Medicine and Biology Society*, pages 1746–1749. IEEE, 2009.

81. A Reşit Kavsaoğlu, Kemal Polat, and M Recep Bozkurt. A novel feature ranking algorithm for biometric recognition with ppg signals. *Computers in biology and medicine*, 49:1–14, 2014.

82. David N Reshef, Yakir A Reshef, Hilary K Finucane, Sharon R Grossman, Gilean McVean, Peter J Turnbaugh, Eric S Lander, Michael Mitzenmacher, and Pardis C Sabeti. Detecting novel associations in large data sets. *science*, 334(6062):1518–1524, 2011.

83. Yang Xing, Chen Lv, and Dongpu Cao. Personalized vehicle trajectory prediction based on joint time-series modeling for connected vehicles. *IEEE Transactions on Vehicular Technology*, 69(2):1341–1352, 2019.

84. Mervyn Stone. Cross-validatory choice and assessment of statistical predictions. *Journal of the Royal Statistical Society: Series B (Methodological)*, 36(2):111–133, 1974.

85. Gavin C Cawley and Nicola LC Talbot. On over-fitting in model selection and subsequent selection bias in performance evaluation. *Journal of Machine Learning Research*, 11(Jul):2079–2107, 2010.

86. Md Rezwanul Haque, Md Milon Islam, Hasib Iqbal, Md Sumon Reza, and Md Kamrul Hasan. Performance evaluation of random forests and artificial neural networks for the classification of liver disorder. In *2018 International Conference on Computer, Communication, Chemical, Material and Electronic Engineering (IC4ME2)*, pages 1–5. IEEE, 2018.

87. J Martin Bland and Douglas G Altman. Statistical methods for assessing agreement between two methods of clinical measurement. *International journal of nursing studies*, 47(8):931–936, 2010.

88. Xiaoqing Yi, Gang Li, and Ling Lin. Noninvasive hemoglobin measurement using dynamic spectrum. *Review of scientific instruments*, 88(8):083109, 2017.

89. Li Gang, Xiong Chan, Wang Hui-quan, Lin Ling, Zhang Bao-ju, and Tong Ying. Single-trial estimation of dynamic spectrum. *SPECTROSCOPY AND SPECTRAL ANALYSIS*, 31(7):1857–1861, 2011.

90. Wei Tang, Qiang Chen, Wenjuan Yan, Guoquan He, Gang Li, and Ling Lin. An optimizing dynamic spectrum differential extraction method for noninvasive blood component analysis. *Applied spectroscopy*, 74(1):23–33, 2020.

91. Gang Li, Sijia Xu, Mei Zhou, Qirui Zhang, and Ling Lin. Noninvasive hemoglobin measurement based on optimizing dynamic spectrum method. *Spectroscopy Letters*, 50(3):164–170, 2017.

92. Ralph WCGR Wijshoff, Massimo Mischi, and Ronald M Aarts. Reduction of periodic motion artifacts in photoplethysmography. *IEEE Transactions on Biomedical Engineering*, 64(1):196–207, 2016.

93. Peter Mell, Tim Grance, et al. The nist definition of cloud computing. 2011.

94. Anjana Luke, Shereena Shaji, and Unnikrishna Menon. Performance enhancement of a photoplethysmographic biosensor using efficient signal processing techniques. In *2018 3rd International Conference for Convergence in Technology (I2CT)*, pages 1–6. IEEE, 2018.

Appendix

A. Data Collection

The fingertip video was filmed during the routine checkup of the patients at the Medical Centre Hospital, 953, O.R. Nizam Road, Chattogram, Bangladesh. The authorities and medical teams approved the study at the Medical Centre Hospital. All the subjects were informed of the entire procedure and provided written consent before the data recording. The full dataset is reported in Table A.1.

Table A.1: Patients information with their clinical data

SL No.	Age	Gender	Video Data	Hb	Gl
01	34	F		11.9	4.44
02	22	F		12.1	6.61
03	23	M		14.3	6.55
…	…	…	…	…	…
…	…	…	…	…	…
…	…	…	…	…	…
92	27	F		13.0	5.80
93	34	F		12.9	10.8

* = Video

B. Data Collection Protocal

- Initially, we received permission from the Department of CSE, KUET, Khulna, Bangladesh.
- We applied for permission for data collection from the Medical Centre Hospital.
- The medical authority examined our device and data collection procedure. With the medical authority's approval, we were then allowed to collect the fingertip videos.
- We trained a team from the hospital on the procedure to collect fingertip data. As an example, we collected fingertip video data from five individuals in front of them.
- Pathologists and doctors took the blood sample of the patients. Patients whose blood samples met our requirements were asked the question "can we take a fingertip video using a smartphone for research purpose?"
- If the patient agreed to participate in the fingertip video after being informed of the research purpose, the nurse recorded the patient's fingertip video.

Table A.2: Selected PPG signal, corresponding extracted features values, and estimated values using DNN models.

PPG Signal	Features (f_1 to f_{36})							Hb			Gl		
								o_r	$\hat{o}^*$	$\hat{o}^+$	o_r	$\hat{o}^*$	$\hat{o}^+$
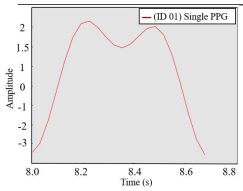	2.32	1.27	0.02	1.95	0.08	2.04	0.98	11.9	12.2	11.92	4.44	4.15	4.37
	0.11	0.04	0.06	0.08	5.0	-1.29	298						
	-97.5	80.1	-308	64.6	-110	-111	0.02						
	0.04	0.06	0.09	0.05	0.02	0.08	9.38						
	1.39	21.1	1.17	31.6	0.51	1.47	34						
	0.0												
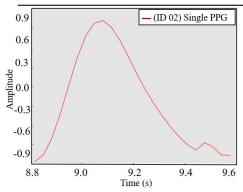	0.85	0.47	0.02	-0.62	0.1	-0.54	-0.62	12.1	11.87	11.79	6.61	6.25	7.12
	0.12	0.04	0.1	0.1	7.0	0.04	64.9						
	-38.8	16.5	-18.48	4.12	-23.0	28.6	0.02						
	0.06	0.1	0.1	0.06	0.03	0.09	9.38						
	0.38	19.92	0.14	28.91	0.07	0.86	22						
	0.0												
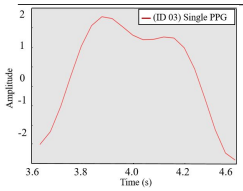	1.93	1.06	0.02	0.39	0.08	0.45	0.27	14.3	14.1	14.47	6.55	4.9	5.71
	0.13	0.04	0.06	0.08	5.0	6.65	263						
	-94.7	18.3	-85.1	38.5	-99.2	-21.1	0.02						
	0.04	0.06	0.1	0.05	0.02	0.08	8.59						
	0.87	17.9	0.76	26.5	0.38	1.39	23						
	1.0												

* o_r = reference value , $\hat{o}^*$ = estimated value with DNN model with all features and $\hat{o}^+$ estimated value with DNN model with MIC selected features.

C. Butterworth Filter

Butterworth filter make the frequency response of a signal as flat as possible in the passband. It is called maximally flat filter because it does not have any ripple in the passband or the stopband. It can be used as highpass, lowpass, or bandpass filter. Luke et al. used an algorithm consists of both butterworth low pass filtering and wavelet transform to remove motion artifacts from PPG data [94]. For a input X, output Y and order n, the factored form Butterworth filter is given by:

$$Butt_n(X) = Y = a_n X^n + a_{n-1} X^{n-1} + a_{n-2} X^{n-2} + \ldots + a_1 X + a_0 \tag{C..1}$$

a_6	a_5	a_4	a_3	a_2	a_1	a_0	n
					1	1	1
				1	$\sqrt{2}$	1	2
			1	2	2	1	3
		1	2.613	3.414	2.613	1	4
	1	3.236	5.236	5.236	3.236	1	5
1	3.864	7.464	9.141	7.464	3.864	1	6

In our case, we used **butter()** function of **'scipy'** library (in python programming language) for Butterworth filter in the implementation.

D. Discrete Fourier Transform

A fast Fourier transform (FFT) is an efficient algorithm to compute the discrete Fourier transform. Fourier transform For X length of n are defined as follows:

$$Y(k) = \sum_{j=1}^{n} X(j) W_n{}^{(j-1)(k-1)} \tag{D..2}$$

where
$W_n = e^{(-2\pi i)/n}$

Let: $X = x_0, x_1, x_2, x_3$ then the out sequence can be represented as below:

$$\begin{bmatrix} Y(0) \\ Y(1) \\ Y(2) \\ Y(3) \end{bmatrix} = \begin{bmatrix} 1 & 1 & 1 & 1 \\ 1 & e^{-j(2\pi/N)} & e^{-j(4\pi/N)} & e^{-j(6\pi/N)} \\ 1 & e^{-j(4\pi/N)} & e^{-j(8\pi/N)} & e^{-j(12\pi/N)} \\ 1 & e^{-j(6\pi/N)} & e^{-j(12\pi/N)} & e^{-j(18\pi/N)} \end{bmatrix} * \begin{bmatrix} x_0 \\ x_1 \\ x_2 \\ x_3 \end{bmatrix}$$

Then, $Y(0)$ contains the zero-frequency term (fundamental component), $Y(1)$ contains the 2^{nd} component, $Y(2)$ contains the 3^{rd} component, $Y(3)$ contains the 4^{th} component.
In our case, we used **ftt()** function of **'numpy'** library (in python programming language) for discrete Fourier transform in the implementation.